

Technical note: Two-component electrical-conductivity-based hydrograph separation employing an exponential mixing model (EXPECT) provides reliable high-temporal-

Original

Technical note: Two-component electrical-conductivity-based hydrograph separation employing an exponential mixing model (EXPECT) provides reliable high-temporal-resolution young water fraction estimates in three small Swiss catchments / Gentile, Alessio; von Freyberg, Jana; Gisolo, Davide; Canone, Davide; Ferraris, Stefano. - In: HYDROLOGY AND EARTH SYSTEM SCIENCES. - ISSN 1607-7938. - ELETTRONICO. - 28:8(2024), pp. 1915-1934. [10.5194/hess-28-1915-2024]

Availability:

This version is available at: 11583/2988321 since: 2024-05-08T11:58:18Z

Publisher:

Copernicus GmbH

Published

DOI:10.5194/hess-28-1915-2024

Terms of use:

This article is made available under terms and conditions as specified in the corresponding bibliographic description in the repository

Publisher copyright

(Article begins on next page)



Technical note: Two-component electrical-conductivity-based hydrograph separation employing an exponential mixing model (EXPECT) provides reliable high-temporal-resolution young water fraction estimates in three small Swiss catchments

Alessio Gentile^{1,2}, Jana von Freyberg^{3,4}, Davide Gisolo^{1,2}, Davide Canone^{1,2}, and Stefano Ferraris^{1,2}

¹Interuniversity Department of Regional and Urban Studies and Planning (DIST),
Polytechnic University of Turin, 10125 Turin, Italy

²Interuniversity Department of Regional and Urban Studies and Planning (DIST),
University of Turin, 10125 Turin, Italy

³School of Architecture, Civil and Environmental Engineering, EPFL, 1015 Lausanne, Switzerland

⁴Mountain Hydrology and Mass Movements, Swiss Federal Institute for Forest,
Snow and Landscape Research (WSL), 8903 Birmensdorf, Switzerland

Correspondence: Alessio Gentile (alessio.gentile@polito.it)

Received: 7 August 2023 – Discussion started: 5 September 2023

Revised: 11 March 2024 – Accepted: 12 March 2024 – Published: 2 May 2024

Abstract. The young water fraction represents the portion of water molecules in a stream that have entered the catchment relatively recently, typically within 2–3 months. It can be reliably estimated in spatially heterogeneous and non-stationary catchments from the amplitude ratio of seasonal isotope ($\delta^{18}\text{O}$ or $\delta^2\text{H}$) cycles of stream water and precipitation, respectively. Past studies have found that young water fractions increase with discharge (Q), thus reflecting the higher direct runoff under wetter catchment conditions. The rate of increase in the young water fraction with increasing Q , defined as the discharge sensitivity of the young water fraction (S_d^*), can be useful for describing and comparing catchments' hydrological behaviour. However, the existing method for estimating S_d^* , which only uses biweekly isotope data, can return highly uncertain and unreliable S_d^* when stream water isotope data are sparse and do not capture the entire flow regime. Indeed, the information provided by isotope data depends on when the respective sample was taken. Accordingly, the low sampling frequency results in information gaps that could potentially be filled by using additional tracers sampled at a higher temporal resolution.

By utilizing high-temporal-resolution and cost-effective electrical conductivity (EC) measurements, along with information obtainable from seasonal isotope cycles in stream

water and precipitation, we develop a new method that can estimate the young water fraction at the same resolution as EC and Q measurements. These high-resolution estimates allow for improvements in the estimates of the S_d^* . Our so-called EXPECT (Electrical-Conductivity-based hydrograph separation employing an EXPponential mixing model) method is built upon the following three key assumptions:

1. We construct a mixing relationship consisting of an exponential decay of stream water EC with increasing young water fraction. This has been obtained based on the relationship between flow-specific young water fractions and EC.
2. We assume that the two-component EC-based hydrograph separation technique, using the above-mentioned exponential mixing model, can be used for a time-source partitioning of stream water into young (transit times < 2–3 months) and old (transit times > 2–3 months) water.
3. We assume that the EC value of the young water end-member (EC_{yw}) is lower than that of the old water end-member (EC_{ow}).

Selecting reliable values from measurements of EC_{yw} and EC_{ow} to perform this unconventional EC-based hydrograph separation is challenging, but the combination of information derived from the two tracers allows for the estimation of endmembers' values. The two endmembers have been calibrated by constraining the unweighted and flow-weighted average young water fractions obtained with the EC-based hydrograph separation to be equal to the corresponding quantities derived from the seasonal isotope cycles.

We test the EXPECT method in three small experimental catchments in the Swiss Alptal Valley using two different temporal resolutions of Q and EC data: sampling resolution (i.e. we only consider Q and EC measurements during dates of isotope sampling) and daily resolution. The EXPECT method has provided reliable young water fraction estimates at both temporal resolutions, from which a more accurate discharge sensitivity of the young water fraction (S_d^{EXP}) could be determined compared with the existing approach. Also, the method provided new information on EC_{yw} and EC_{ow} , yielding calibrated values that fall outside the range of measured EC values. This suggests that stream water is always a mixture of young and old water, even under very high or very low wetness conditions. The calibrated endmembers revealed a good agreement with both endmembers obtained from an independent method and EC measurements from groundwater wells.

For proper use of the EXPECT method, we have highlighted the limitations of EC as a tracer, identified certain catchment characteristics that may constrain the reliability of the current method and provided recommendations about its adaptation for future applications in catchments other than those investigated in this study.

1 Introduction

Environmental tracers in catchment studies are used to understand the age, origin and pathways of water in natural environments (Kendall and McDonnell, 1998). Among tracers, hydrologists use the stable water isotopes (^{18}O and 2H) because they are a constituent part of water molecules and, thus, are naturally present in precipitation (Kendall and McDonnell, 1998). The isotopic composition of precipitation (C_P) generally shows a pronounced seasonal cycle (Dansgaard, 1964). Catchment storage acts as a filter on this seasonal input cycle, so that the isotope cycle in stream water (C_S) is damped and lagged compared with that of precipitation (McGuire and McDonnell, 2006). The delay and damping that we observe in the stream water cycle is caused by the advection and dispersion of stable water isotopes that reach the catchment with precipitation, thus reflecting water mixing as well as the diversity of flow paths and their velocities (Kirchner, 2016a; McGuire and McDonnell, 2006).

Kirchner (2016a, b) proposed a new water age metric directly related to the amplitude ratio of the seasonal isotope cycles in stream water and precipitation: the young water fraction, i.e. the portion of runoff younger than roughly 2–3 months. The precipitation isotope cycle amplitude (A_P) is generally estimated via a robust fit of a sine function to the isotopic composition of precipitation samples using the precipitation amount associated with each sample as the weight to reduce the influence of low-precipitation events (von Freyberg et al., 2018a; Kirchner, 2016a). The stream water isotope cycle amplitude is estimated via a robust fit of a sine function to the isotopic composition of stream water samples with or without using discharges (Q) at the sampling times as weights (von Freyberg et al., 2018a). Please note that, hereafter, the symbol “*” indicates a streamflow-weighted variable. Therefore, it is necessary to distinguish between the unweighted and the flow-weighted stream water amplitude (A_S and A_S^* , respectively; see Eq. (S2) for further details) and, accordingly, between the unweighted and the flow-weighted young water fraction (F_{yw} and F_{yw}^* , respectively).

Recently, Gallart et al. (2020b) proposed a method to estimate the rate of increase in the young water fraction with increasing Q by fitting the sinusoid function, with amplitude $A_S^*(Q) = A_P F_{yw}^*(Q)$, directly to the isotopic data of stream water as follows:

$$\begin{aligned} C_S(Q, t) &= A_S^*(Q) \sin(2\pi ft - \varphi_S^*) + k_S^* \\ &= A_P \left[F_{yw}^*(Q) \right] \sin(2\pi ft - \varphi_S^*) + k_S^* \\ &= A_P \left[1 - (1 - F_0^*) \exp(-Q S_d^*) \right] \\ &\quad \sin(2\pi ft - \varphi_S^*) + k_S^*, \end{aligned} \quad (1)$$

where the F_0^* , S_d^* , φ_S^* and k_S^* parameters are obtained via non-linear fitting (see “The discharge sensitivity of young water fraction” section in the Supplement for additional methodological details). The S_d^* ($d\ mm^{-1}$) parameter is defined as the discharge sensitivity of the young water fraction, F_0^* (–) is the virtual young water fraction when $Q = 0$, φ_S^* (rad) is the phase of the seasonal cycle, f is the frequency (equal to once per year for a seasonal cycle) and k_S^* (‰) is a constant representing the vertical offset of the seasonal cycle. Referring to the expression enclosed in square brackets in Eq. (1), the young water fraction is assumed to vary with discharge following an exponential-type equation that converges toward 1 at the highest flows but that does not converge toward 0 at the lowest flows, thus theoretically admitting $F_0^* < 0$. Because of this mathematical relationship between the young water fraction and Q , young water fraction time series can, in theory, be calculated at the same temporal resolution as Q . However, the uncertainties in such time series can be substantial because the underlying isotope data, due to the low sampling frequency, are generally not able to capture the entire range of flow regimes, especially the (very) high flow rates (Xia et al., 2023). This becomes evident in Figs. 1 and 3 of Gallart et al. (2020b), where the stan-

dard errors of flow-specific F_{yw} are largest during the highest flows. From these considerations emerges the need for a new method to reliably estimate the time series of young water fractions and to better constrain the discharge sensitivity of young water fractions under very low and very high flow conditions.

Multiyear stable water isotope data sets are typically available at relatively low (e.g. biweekly or monthly) temporal resolutions because of the high cost of sampling and laboratory analysis (Mosquera et al., 2018). For the same reasons, high-resolution isotopic data sets are often limited to relatively short time windows (Wang et al., 2019). However, the information provided by isotope data depends on when the respective samples were taken (Wang et al., 2019). Consequently, sampling at low temporal resolution results in information gaps that could potentially be filled by using additional tracers sampled at higher temporal resolution. As a tracer, electrical conductivity (EC), which is a bulk measure of the major ions in water (Riazi et al., 2022), can be measured over extended periods at high temporal resolution, while the cost of installation and maintenance remains low (Cano-Paoli et al., 2019; Mosquera et al., 2018). However, EC is not a conservative tracer (like stable water isotopes) because it is affected by geochemical reactions and the dissolution of reactive solutes in stream water (Cano-Paoli et al., 2019; Benettin et al., 2022). Because of these characteristics, the EC and stable water isotope tracers complement each other well and, thus, can be jointly used to constrain model parameterizations and to inform transit time models (Cano-Paoli et al., 2019; Benettin et al., 2022).

A time-source separation is generally performed using isotope hydrograph separation, IHS (Klaus and McDonnell, 2013), while major ions (approximated by EC) have been previously used for geographic-source separation in end-member mixing analysis (Hooper, 2003; Penna et al., 2017). Major ions' concentration in stream water derives from mineral weathering. Weathering processes can be viewed as a series of geochemical reactions influenced by the characteristics of fluid movement, such as the contact time between the flowing water and mineral surfaces (Benettin et al., 2015, 2017). Thus, the longer a water particle remains within the subsurface, the higher its solute concentration (and thus EC) will be once it is released as streamflow (Benettin et al., 2017). Indeed, Mosquera et al. (2016), investigating the mean transit time (MTT) of water and its spatial variability in the wet Andean páramo, found that the mean EC is an efficient predictor of mean transit time in this high-elevation tropical ecosystem. More recently, Riazi et al. (2022), modelling EC variation using a travel time distribution approach, assumed that the salinity of water in catchment storages is a function of water age. Bonacci and Roje-Bonacci (2023) used EC measurements of a karst spring to estimate the time that water spent in the karst aquifer. In addition, Kirchner (2016b) stated that the concentration of reactive chemical species, such as EC, can be used to construct a mixing rela-

tionship with the young water fraction, which provides information about the water age. Overall, these studies suggest that EC may provide useful information on water age (Riazi et al., 2022). Indeed, past studies have used EC for time-source hydrograph separation (HS) in event and pre-event water with promising results that favourably compare with those obtained from conservative tracers (Riazi et al., 2022). For instance, Laudon and Slaymaker (1997), applied HS in two small nested alpine/subalpine catchments using different tracers ($\delta^{18}\text{O}$, $\delta^2\text{H}$, EC and silica) and returned generally comparable results overall. Cey et al. (1998), with the aim of quantifying groundwater discharge in a small agricultural watershed, separated the hydrograph into event and pre-event water (assumed to be groundwater), obtaining only slightly different results utilizing $\delta^{18}\text{O}$ and EC. Pellerin et al. (2008) performed HS on 19 low- to moderate-intensity rainfall events in a small urban catchment via the use of EC, silica and $\delta^2\text{H}$, obtaining a similar outcome regardless of the tracer used. In a similar environment, Meriano et al. (2011) revealed a high level of agreement between flow partitioning results during a midsummer event using HS with $\delta^{18}\text{O}$ and EC as tracers. Camacho Suarez et al. (2015), to identify the mechanisms of runoff in a semi-arid catchment, applied HS using both EC and $\delta^{18}\text{O}$ and found no major disadvantages when using EC. More recently, Mosquera et al. (2018) used the TraSPAN model to simulate storm flow partitioning in a forested temperate catchment, revealing similar portions of pre-event water regardless of the tracer ($\delta^{18}\text{O}$ and EC) used. Cano-Paoli et al. (2019), by investigating the stream-flow separation into event and pre-event components in an alpine catchment, obtained consistent results using $\delta^{18}\text{O}$, $\delta^2\text{H}$ and EC. Lazo et al. (2023) showed that, in a tropical alpine catchment, the use of EC returned similar results for event and pre-event water to those obtained with $\delta^{18}\text{O}$ for a wide range of flow conditions reflected by the 37 monitored rainfall–runoff events. Overall, the findings of these studies suggest a quasi-conservative behaviour of EC under a wide range of hydrological and lithological conditions, even if its behaviour depends on specific characteristics (e.g. water partitioning between the surface and the subsurface, spatial distribution of minerals and subsurface properties, kinetics of rock dissolution, and individual ion concentrations) of each watershed (Laudon and Slaymaker, 1997; Benettin et al., 2022; Lazo et al., 2023). Nevertheless, these studies have been limited to the comparison of results obtained by applying HS with different tracers and did not integrate the information obtainable from stable water isotopes and EC to generate new insights into transit times, hydrological processes, or the links between water quality and water age variations (Benettin et al., 2017, 2022).

In this regard, here we develop a new multi-tracer method that combines biweekly stable water isotope data ($\delta^{18}\text{O}$) with EC measurements. This study aims to both reduce the standard error of S_d^* and estimate the young water fraction at a

temporal resolution higher than 2 weeks, which will lead to new insights into the catchments under study.

2 Material and methods

2.1 Study sites and the data set

To test the applicability of our method (Sect. 2.2), we use data from the Erlenbach (ERL), Lümpenbach (LUE) and Vogelbach (VOG) catchments, located in the pre-alpine Alptal Valley in central Switzerland. The geographical framework of the three study sites is reported in Fig. 1.

The three study catchments cover areas of between 0.7 and 1.6 km², and mean elevation ranges from 1335 to 1359 m a.s.l. (metres above sea level; Table 1, Fig. 1a). Mean catchment slopes are 13.53, 12.49 and 18.42° in the ERL, LUE and VOG catchments, respectively, but the hillslopes can be much steeper locally (20–40°) (Stähli et al., 2021). According to the swissTLMRegio model (Fig. 1c), the ERL catchment is mainly constituted by forest (45 %) and swamp-land (49 %); these are also the dominant classes in the LUE (21 % and 39 %, respectively) and VOG (72 % and 13 %, respectively) catchments. Most of the southern Alptal Valley is characterized by shallow, low-permeability Gleysols that limit the deep infiltration of water and lead to shallow groundwater tables (Stähli et al., 2021). The percentage of soils with a low storage capacity is about 4 % in both ERL and LUE, while it is 51 % in the VOG catchment; a large fraction of the soils is saturated (≥ 95 % in ERL and LUE and 49 % in VOG; von Freyberg et al., 2018a). The geological substratum of the three study sites consists mainly of sedimentary rock (flysch). The catchment area that is covered by Quaternary deposits is much higher in the ERL and LUE catchments than in the VOG catchment (Table 1). Therefore, although the study catchments are located within close proximity, they differ in terms of soil wetness and unconsolidated sediments.

The average hydro-climatic conditions are generally similar for all three catchments. The average annual precipitation in the period from January 2000 to December 2015, based on interpolated data from the PREVAH model, was about 1853, 1803 and 1800 mm in the ERL, LUE and VOG catchments, respectively (von Freyberg et al., 2018a). The average monthly discharge is similar among the catchments: 138.9, 152.0, and 117.4 mm per month at the ERL, LUE and VOG catchments, respectively (von Freyberg et al., 2018a). These watersheds reveal a hybrid hydro-climatic regime (Staudinger et al., 2017; von Freyberg et al., 2018a), as we observe ephemeral snowpack formation (typically from December to April) that also rapidly melts away during winter, meaning that the snowpack may not last throughout the entire winter season (Stähli et al., 2021).

Daily-resolution Q and stream water EC data have been downloaded from the Swiss Federal Office for Forest, Snow

and Landscape Research (WSL, Birmensdorf, Switzerland) data portal. We have estimated the Q –EC relationships with a log-type fit (Fig. 2). As daily Q increases, daily EC decreases at the three study sites. This pattern arises due to the contribution of different sources (i.e. ages) of water to the stream. At the three study sites, stream discharge increases due to rainfall or snowmelt, which are generally low in EC, resulting in a dilution of stream water EC. In addition, during wet conditions (high Q), more rapid flow paths are activated, leading to a prevalence of the younger hydrograph component. Because of the short interaction time with mineralized rocks and soils, young water can be assumed to be low in dissolved ions (i.e. low EC). The other extreme, low Q and high stream water EC, occurs during baseflow conditions when the stream is mainly fed by old (i.e. highly mineralized and high-EC) subsurface water (Schmidt et al., 2012).

This study uses F_{yw} , F_{yw}^* , F_{yw}^Q and S_d^* (Tables 2, 4), which have been estimated in past studies (Gallart et al., 2020b; von Freyberg et al., 2018a) by considering streamflow $\delta^{18}O$ data from biweekly grab sampling over a period of approximately 5 years for the three study catchments. F_{yw}^Q values refer to young water fractions estimated in discrete flow regimes (Kirchner, 2016b). Indeed, it is possible to separate the stream water isotope data collected into different discharge ranges and fit sinusoids separately to the isotope content in each range. For each of these individual flow regimes, this method enables one to obtain the stream water seasonal isotope cycles amplitude (A_S^Q) values that will be divided by A_P to obtain F_{yw}^Q (von Freyberg et al., 2018a; Kirchner, 2016b). For more details about F_{yw}^Q estimation, the reader is referred to Kirchner (2016b) and von Freyberg et al. (2018a).

2.2 The EXPECT method: two-component electrical-conductivity-based hydrograph separation employing an exponential mixing model

The young water fraction may be useful for inferring chemical processes from streamflow concentrations of reactive chemical species (Kirchner, 2016b). Indeed, as it is known how the fraction of young water varies in discrete flow regimes, it is possible to construct mixing relationship between F_{yw}^Q and the concentration of reactive chemical species (Kirchner, 2016b). Accordingly, we calculate the median EC within each individual discharge range (reported in Table 2), and we investigate how the median EC varies with F_{yw}^Q (Fig. 3).

As visible in Fig. 3, the relationship between F_{yw}^Q and median-flow-specific EC is well described by an exponential mixing model. Indeed, the widely used linear mixing model proves to be poorly suited here because it is pointing to a negative EC endmember of young water (i.e. EC value corresponding to $F_{yw}^Q = 1$; Fig. 3). This will be thoroughly discussed in Appendix A. By considering the exponential mixing model, we can estimate the “idealized” old water and young water endmembers via evaluation of the fitted expo-

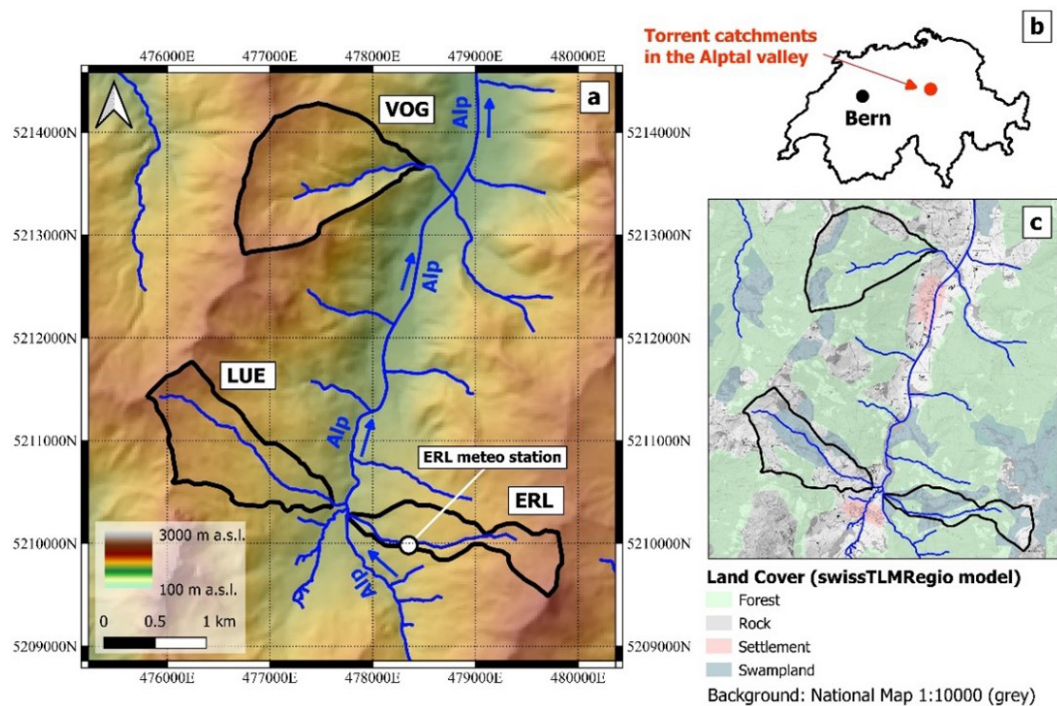


Figure 1. (a) Location of the three study catchments with indication of the stream networks and elevation (DHM25 © swisstopo) as background. The Alp River is marked in the map with blue arrows indicating its flow direction. (b) Location of the Alptal Valley in Switzerland. (c) Land cover of the three study catchments from the swissTLMRegio 2D landscape model (© swisstopo).

Table 1. Topographic, geological and hydro-climatic properties of the three study sites.

ID	ERL	LUE	VOG
Area (km ²) ^a	0.7	0.9	1.6
Mean elevation (range) (m a.s.l.) ^a	1359 (1117–1650)	1336 (1092–1508)	1335 (1038–1540)
Mean slope (°) ^b	13.53	12.48	18.42
Saturated soils (%) ^a	0.95	0.96	0.49
Geological substratum ^b	Sed. rock (flysch)	Sed. rock (flysch)	Sed. rock (flysch)
Areal fraction of Quaternary deposits (–) ^b	0.74	0.9	0.48
Regime (Staudinger et al., 2017) ^a	hybrid	hybrid	hybrid
Average precipitation (mm per month) ^a	162.4	157.1	162.2
Average discharge (mm per month) ^a	138.9	152	117.3
Period of isotope sampling ^a	Jul 2010–May 2015	Oct 2010–Nov 2015	Jun 2010–Nov 2015

^a Data published in von Freyberg et al. (2018a). ^b Data published in Gentile et al. (2023).

nential expressions for $F_{yw}^Q = 0$ and $F_{yw}^Q = 1$, respectively. Accordingly, a first-order estimate of the two endmembers (EC_{ow}^{raw} , EC_{yw}^{raw} , respectively) is reported in Fig. 3 and Table 3. It is evident that the measured F_{yw}^Q for the three study catchments ranges from approximately 0.1 to 0.5 (Fig. 3). As the measurable range of young water fractions is not wide enough, the parameters estimated with the exponential fit are highly uncertain because the curve is poorly constrained at very low (< 0.1) and very high (> 0.5) young water fractions. In this regard, hereafter, we propose a new methodology to estimate the EC endmembers of young and old water,

respectively, and to perform a continuous hydrograph separation with an alternative mixing model.

The definition of the fraction of the streamflow younger than a threshold age (varying modestly from 2 to 3 months) at the generic time t_i , $F_{yw}(t_i)$, implicitly defines the existence of a complementary fraction of streamflow older than that threshold age at the same time t_i , $F_{ow}(t_i)$. Thus, mass conservation requires the following:

$$F_{yw}(t_i) + F_{ow}(t_i) = 1. \quad (2)$$

Table 2. Young water fractions of distinct flow regimes (F_{yw}^Q) as well as average unweighted and flow-weighted young water fractions (F_{yw} and F_{yw}^* , respectively) with the corresponding standard error (SE) values. The number of samples used to estimate F_{yw}^Q alongside the median Q and EC of each flow regime are also reported. These data, excluding the median EC, were previously obtained by von Freyberg et al. (2018a).

Catchment ID	Q (range)	No. samples	Median Q (mm d ⁻¹)	Median EC (μS cm ⁻¹)	$F_{yw}^Q \pm \text{SE}$	$F_{yw} \pm \text{SE}$	$F_{yw}^* \pm \text{SE}$
ERL	Q (0 %–25 %)	35	0.42	274.68	0.294 ± 0.039	0.37 ± 0.03	0.49 ± 0.03
	Q (25 %–50 %)	35	0.93	248.71	0.353 ± 0.032		
	Q (50 %–75 %)	35	2.21	213.28	0.449 ± 0.049		
	Q (75 %–100 %)	35	7.23	163.21	0.467 ± 0.048		
	Q (80 %)	28	8.20	157.18	0.446 ± 0.061		
	Q (90 %)	14	19.21	148.51	0.52 ± 0.083		
LUE	Q (0 %–25 %)	33	1.11	298.95	0.189 ± 0.024	0.25 ± 0.02	0.33 ± 0.03
	Q (25 %–50 %)	33	1.81	287.73	0.205 ± 0.029		
	Q (50 %–75 %)	33	3.56	266.39	0.363 ± 0.039		
	Q (75 %–100 %)	33	7.68	210.88	0.356 ± 0.051		
	Q (80 %)	27	9.16	205.84	0.35 ± 0.057		
	Q (90 %)	14	12.59	192.03	0.403 ± 0.075		
VOG	Q (0 %–25 %)	35	0.73	234.97	0.163 ± 0.02	0.21 ± 0.02	0.31 ± 0.02
	Q (25 %–50 %)	35	1.11	217.55	0.168 ± 0.024		
	Q (50 %–75 %)	34	2.22	193.28	0.267 ± 0.034		
	Q (75 %–100 %)	35	7.80	148.08	0.316 ± 0.039		
	Q (80 %)	28	8.65	142.19	0.325 ± 0.044		
	Q (90 %)	14	12.13	133.02	0.36 ± 0.051		

Table 3. Optimized endmembers obtained via the EXPECT method. The 1st, 2nd and 3rd quartiles (q_1 , q_2 and q_3 , respectively) and the interquartile range (IQR) of the optimized endmembers’ empirical distribution are also reported. First-order estimates of endmembers derived from the exponential model fitted on median EC vs. F_{yw}^Q (see also Fig. 3) with the related standard error (SE) values are reported on the right-hand side of this table. Values are in μS cm⁻¹.

Time resolution	ID	EC_{yw}^{opt}	q_1	q_2	q_3	IQR	EC_{ow}^{opt}	q_1	q_2	q_3	IQR	ID	$EC_{yw}^{\text{raw}} \pm \text{SE}$	$EC_{ow}^{\text{raw}} \pm \text{SE}$
Daily (DR)	ERL	54.25	44.28	54.05	63.17	18.89	501.03	446.52	502.47	583.37	136.85	ERL	37.13 ± 62.53	642.42 ± 140.13
	LUE	51.08	37.27	50.67	65.02	27.75	449.79	411.12	450.29	504.31	93.19			
	VOG	29.71	23.79	29.45	35.13	11.34	318.82	300.33	319.92	345.73	45.4			
Sampling (SR)	ERL	44.78	35.88	44.74	53.4	17.52	565.89	495.15	566.39	668.09	172.94	LUE	71.10 ± 139.60	414.13 ± 62.81
	LUE	65.68	49.29	65.18	80.93	31.64	410.43	379.38	410.69	454.26	74.88			
	VOG	32.25	25.64	31.41	37.27	11.63	315.23	299.56	318.53	342.67	43.11			

To estimate $F_{yw}(t_i)$, and thus $F_{ow}(t_i)$, we use EC as a tracer to separate the hydrograph into young (transit time < 2–3 months) and old (transit time > 2–3 months) water. Solid support from the scientific literature justifying the use of EC for time-source hydrograph separation is illustrated in Sect. 1.

As suggested by the analysis reported in Fig. 3, to perform the hydrograph separation, we assume that stream water EC at the generic time t_i , $EC(t_i)$, decreases exponentially with increasing $F_{yw}(t_i)$:

$$EC(t_i) = EC_{ow} e^{-a F_{yw}(t_i)}, \tag{3}$$

where EC_{ow} is the old water EC endmember and a is a parameter. The exponential decay proposed in Eq. (3) guarantees a realistic scenario for the case $F_{yw}(t_i) = 0$, i.e. streamflow contains only old water ($F_{ow}(t_i) = 1$) and stream water EC is equal to EC_{ow} ($EC(t_i) = EC_{ow}$). Conversely, if $F_{yw}(t_i)$ is equal to 1, streamflow is made up entirely of young water. Accordingly, we can include the following condition: if $F_{yw}(t_i) = 1$, $EC(t_i) = EC_{yw}$, where EC_{yw} is the young water EC endmember (Eq. 4),

$$EC_{yw} = EC_{ow} e^{-a}. \tag{4}$$

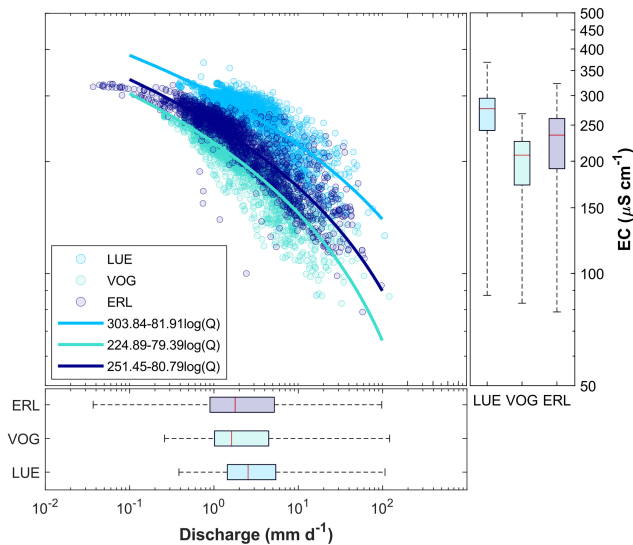


Figure 2. Relation between daily EC and daily Q for the three study sites. As discharge increases, the EC decreases in the three study catchments. This pattern arises mainly due to the age (source) of water contributing to the stream: if a substantial amount of recent, low-EC water contributes to streamflow during rainfall or snowmelt, stream water EC decreases while discharge increases.

Furthermore, we assume $EC_{yw} < EC_{ow}$. Solid support of this assumption from the scientific literature is illustrated in Sect. 3.1 alongside the discussion of the results.

By further considering the law of water mass conservation (Eq. 2), it is possible to solve the system of three equations (Eqs. 2–4) with three variables (a , $F_{yw}(t_i)$ and $F_{ow}(t_i)$), thus obtaining the explicit expression of a (Eq. 5) and, accordingly, of $F_{yw}(t_i)$ (Eq. 6).

$$a = -\ln\left(\frac{EC_{yw}}{EC_{ow}}\right) \quad (5)$$

$$F_{yw}(t_i) = \frac{\ln\left(\frac{EC(t_i)}{EC_{ow}}\right)}{\ln\left(\frac{EC_{yw}}{EC_{ow}}\right)} \quad (6)$$

The main difficulty in applying Eq. (6) to estimate $F_{yw}(t_i)$ is that we generally cannot accurately determine the endmembers EC_{yw} and EC_{ow} from the analysis reported in Fig. 3 or from measurements. Indeed, such endmembers correspond to the (rare) scenarios in which $F_{yw}(t_i)$ is either 0 or 1. The first scenario ($F_{yw}(t_i) = 0$) might occur only after prolonged periods without rainfall or snowmelt, whereas the second scenario ($F_{yw}(t_i) = 1$) is unlikely to occur in most natural catchments where baseflow is usually older than 3 months (Gentile et al., 2023), and thus we cannot directly measure EC_{yw} (Kirchner, 2016b). In this regard, hereafter, we present a novel methodology to estimate the endmembers. Such a methodology lays its foundations on the statement that the isotope-based F_{yw} and F_{yw}^* (Eqs. 7a and 7b; see the Supplement for further details) accurately estimate the un-

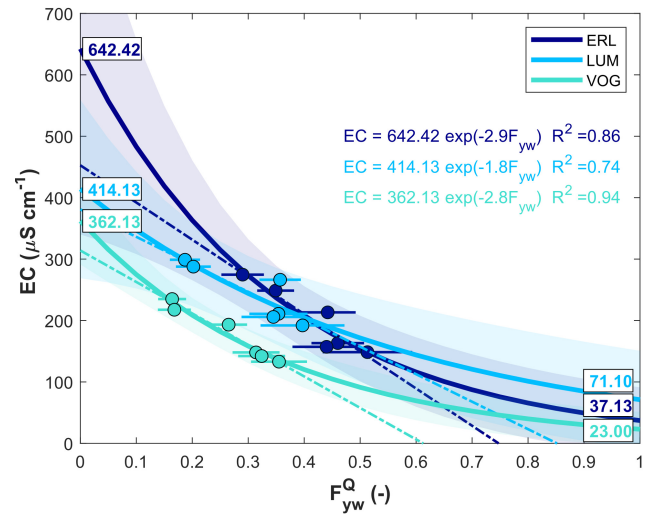


Figure 3. Median-flow-specific EC against F_{yw}^Q for the three study catchments. Horizontal bars indicate the F_{yw}^Q standard error. The solid lines indicate the exponential fits (for which expressions with the corresponding R^2 value are also indicated). The shaded areas indicate the 90 % prediction bounds. The text boxes corresponding to $F_{yw}^Q = 0$ indicate a first-order estimate of old water endmembers (EC_{ow}^{raw}) using the exponential expression. Similarly, the text boxes corresponding to $F_{yw}^Q = 1$ indicate a first-order estimate of young water endmembers (EC_{yw}^{raw}) using the exponential expression. The dashed lines indicate the linear fits to data that point to a negative EC endmember of young water (i.e. EC value corresponding to $F_{yw}^Q = 1$).

weighted and the flow-weighted average young water fractions in streamflow, respectively (Kirchner, 2016b).

$$F_{yw} = \frac{A_S}{A_P} \quad (7a)$$

$$F_{yw}^* = \frac{A_S^*}{A_P} \quad (7b)$$

Accordingly, if we know the young water fraction over a generic time step t_i , $F_{yw}(t_i)$ (e.g. daily young water fraction), we can calculate the unweighted and the flow-weighted average young water fraction in streamflow using Eqs. (8a) and (8b), respectively:

$$\tilde{F}_{yw} = \frac{\sum_{i=1}^n F_{yw}(t_i)}{n} \simeq F_{yw}, \quad (8a)$$

$$\tilde{F}_{yw}^* = \frac{\sum_{i=1}^n Q(t_i) F_{yw}(t_i)}{\sum_{i=1}^n Q(t_i)} \simeq F_{yw}^*, \quad (8b)$$

where n is the number of time steps (e.g. days) in the period of isotope sampling and $Q(t_i)$ is the discharge at the

time t_i (e.g. daily discharge). The hat “~” symbol is simply used to visually differentiate between the average young water fractions obtained with both approaches. Note that Eq. (8b) was previously presented in Gentile et al. (2023).

We therefore determine EC_{yw} and EC_{ow} through calibration, respecting the following three constraints:

- i. EC_{ow} and EC_{yw} are greater than or equal to 0;
- ii. \tilde{F}_{yw} , where $F_{yw}(t_i)$ is obtained using Eq. (6), must match the F_{yw} estimated with the amplitude ratio technique (Eq. 7a);
- iii. \tilde{F}_{yw}^* , where $F_{yw}(t_i)$ is obtained using Eq. (6), must match the F_{yw}^* estimated with the amplitude ratio technique (Eq. 7b).

In summary, we perform a constrained EC-based hydrograph separation in which the two endmembers (EC_{yw} and EC_{ow}) are calibrated through an optimization procedure. Specifically, we use the MATLAB `fmincon` solver, specifically the `sqp` (sequential quadratic programming) algorithm, within the `GlobalSearch` procedure that repeatedly runs the local solver to generate a global solution. To satisfy point (i), we search the endmember values within the range $[0, +\infty)$. We consider ∞ as the upper limit because catchments can also have immobile storages that could potentially never participate to the water cycle (Staudinger et al., 2017). In addition, we calibrate the EC endmembers by minimizing the following objective function, which is designed to satisfy points (ii) and (iii):

$$\text{obj} = \frac{(\tilde{F}_{yw} - F_{yw})^2 + \frac{F_{yw}^*}{\tilde{F}_{yw}} (\tilde{F}_{yw}^* - F_{yw}^*)^2}{\left(1 + \frac{F_{yw}^*}{F_{yw}}\right)}. \quad (9)$$

We give a greater weight to the second term, $(\tilde{F}_{yw}^* - F_{yw}^*)^2$. The weight is proportional to how much higher F_{yw}^* is than F_{yw} , as Gallart et al. (2020a) showed that the flow-weighted analysis produces a less biased estimation of the young water fraction. The outputs of the optimization procedure are the calibrated young water and old water endmembers (EC_{yw}^{opt} and EC_{ow}^{opt} , respectively). Subsequently, we calculate the F_{yw}^{opt} (at every time step t_i) with Eq. (6) by using the optimal endmembers (EC_{yw}^{opt} and EC_{ow}^{opt}), and we plot F_{yw}^{opt} against Q , thereby visualizing an empirical relationship between the two variables. Finally, we fit the expression enclosed in square brackets in Eq. (1) (corresponding to Eq. 6 from Gallart et al., 2020b) to our F_{yw}^{opt} data:

$$F_{yw}^{\text{opt}} = 1 - (1 - F_0^{\text{EXP}}) \exp(-QS_d^{\text{EXP}}). \quad (10)$$

We then compare the discharge sensitivity, S_d^* , previously determined using only stream water isotope data (see Eq. 1), and the discharge sensitivity, S_d^{EXP} , determined from Eq. (10). We further compare our results to the F_{yw}^Q values (Table 2) previously obtained by von Freyberg et al. (2018a).

We apply our method at two different time resolutions that are reflected in our data set: the daily resolution (DR) and the sampling resolution (SR). At the DR, $EC(t_i)$ and $Q(t_i)$ refer to the daily average EC and Q values, respectively; thus, $F_{yw}(t_i)$ is the average young water fraction of each day. At the SR, it should be noted that the “EC samples” are not referring to physical samples in this specific application. Accordingly, $EC(t_i)$ and $Q(t_i)$ are obtained by sub-setting those EC and Q values from the daily time series that correspond to the time of isotope sampling. In this sense, we can say that the number of EC samples and isotope samples is the same. Nevertheless, the method can be potentially applied at the SR in catchments in which EC is only measured from water samples. At the SR, $F_{yw}(t_i)$ values are estimated only for those days on which an isotope sample was taken.

We quantify the uncertainty in EC_{yw}^{opt} and EC_{ow}^{opt} by repeating the global optimization procedure by randomly sampling 10 000 couples of F_{yw} and F_{yw}^* from the intervals $F_{yw} \pm \text{SE}$ and $F_{yw}^* \pm \text{SE}$, respectively. The SE values are reported in Table 2. The random sampling assumes that the values within the two intervals have a Gaussian probability of extraction, thus favouring the sampling of the core values. Therefore, we obtain 10 000 couples of endmembers for which we compute statistics. We further calculate the uncertainty in $F_{yw}^{\text{opt}}(t_i)$: we apply Eq. (6) using the 10 000 couples of endmembers, thus obtaining 10 000 $F_{yw}^{\text{opt}}(t_i)$ values at each time step t_i , for which we calculate the standard deviation.

It should be noted that the initial conceptualization of the mixing model was based on testing the hydrograph separation using the two-component endmember linear mixing approach with EC as the tracer (e.g. Cano-Paoli et al., 2019). As could already be inferred from Fig. 3, this approach was not successful because it can represent only a limited hydrological behaviour of catchments that does not capture that of our three study catchments. A detailed explanation of the limits regarding the linear mixing model is provided in Appendix A of this paper.

Last but not least, as our method consists of a two-component Electrical-Conductivity-based hydrograph separation employing an EXponential mixing model, we decide to name it EXPECT. A schematic representation of the EXPECT method is reported in Fig. 4.

3 Results and discussion

3.1 Physical likelihood of calibrated endmembers and the discharge sensitivity of the young water fraction

The application of the EXPECT method showed, at both the daily and sampling resolutions, that the old water EC endmembers, EC_{ow}^{opt} , are about 1 order of magnitude larger than the young water EC endmembers, EC_{yw}^{opt} , for all three experimental catchments (Table 3, Fig. 5). This result can be explained by considering that old water had a longer contact

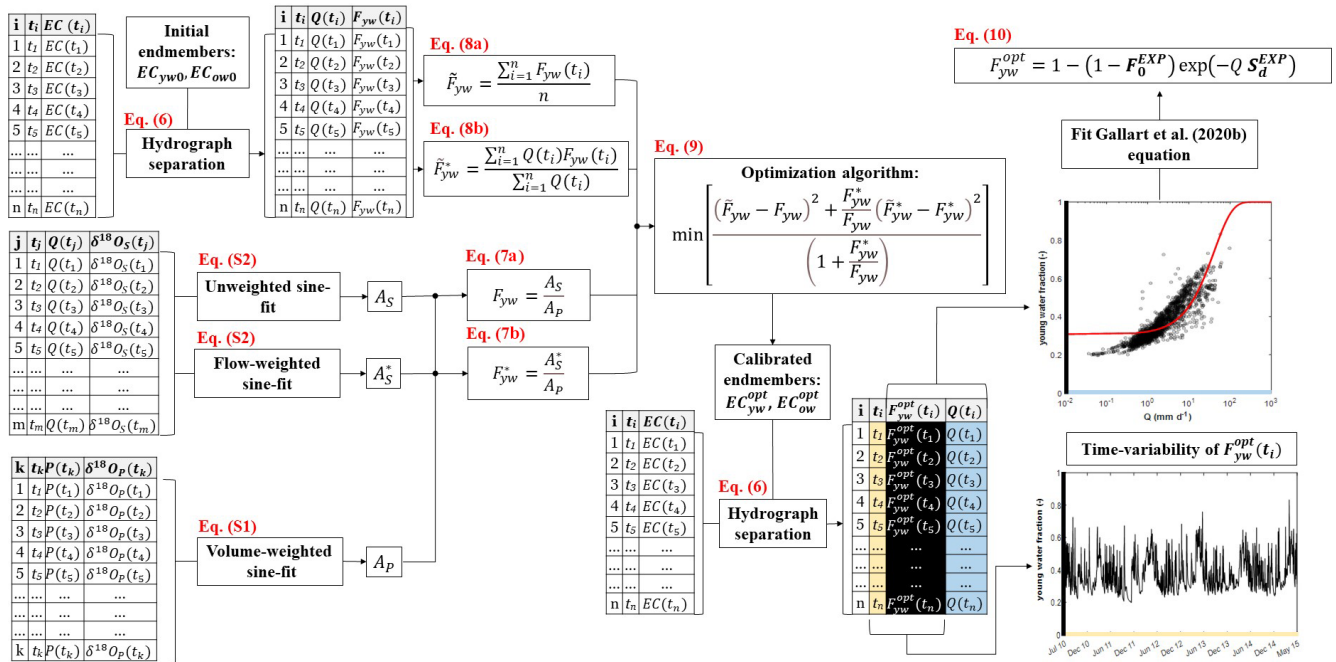


Figure 4. Schematic representation of the EXPECT method. The subscript “P” refers to precipitation, while the subscript “S” refers to stream water. $P(t_k)$ indicates the volume of precipitation used for the volume-weighted fit of precipitation isotopes ($\delta^{18}O_P(t_k)$). The sampling times of $EC(t_i)$, $Q(t_i)$, $\delta^{18}O_S(t_j)$ and $\delta^{18}O_P(t_k)$ may not be aligned; consequently, the time series typically have different lengths. Thus, the times t_i , t_j and t_k have different indices and usually $n \neq m \neq k$.

period with mineral surfaces in the subsurface (Benettin et al., 2015, 2017); thus, weathering-derived solute concentrations (and, correspondingly, EC) will be higher in old water compared with young water. Moreover, young and old stream water components can originate from different reservoirs in a catchment (Riazi et al., 2022). Among these reservoirs, old water is generally assumed to represent groundwater. This is also supported by the fact that the fraction of baseflow (representing the groundwater contribution to streamflow) was found to be complementary to the young water fraction in the framework (including the three Swiss catchments in this study) investigated by Gentile et al. (2023). In this regard, different papers that have characterized groundwater EC have shown notable differences with the EC of precipitation and/or meltwater. Indeed, Zuecco et al. (2018), by investigating the hydrological processes in an alpine catchment, found that the EC of rainwater and of recent snow was 19.2 and 12.2 $\mu\text{S cm}^{-1}$, respectively. Conversely, they found that groundwater from springs had an EC of 166 $\mu\text{S cm}^{-1}$. Moreover, by investigating the conceptualization of meltwater dynamics in an alpine catchment through hydrograph separation, Penna et al. (2017) defined the snowmelt endmember range as 2.9–15.3 $\mu\text{S cm}^{-1}$, the glacier melt endmember range as 2–2.7 $\mu\text{S cm}^{-1}$ and the groundwater endmember range as 210–317.7 $\mu\text{S cm}^{-1}$ (average values from springs or streams in fall/winter). These examples are intended to show that groundwater (the main source of old water) gen-

erally reveals an EC value that is much higher (around 10- to 100-fold) than other sources in a catchment that should preferentially contribute to the young stream water component. Differences in young and old water EC endmembers can also be partially justified by looking at differences in event and pre-event water EC endmembers. Indeed, old (transit times > 2–3 months) water is a large fraction of pre-event (transit times > a few days) water, whereas event water (transit times < a few days) is a portion of young water (transit times < 2–3 months). Due to this overlap, a similarity in the old water and pre-event water EC endmembers or in the young water and event water EC endmembers would not be surprising. Cano-Paoli et al. (2019) used stream water EC to investigate hydrological processes in alpine headwaters by separating the hydrograph into event and pre-event water. In this regard, they defined the event water endmember as being equal to 8 $\mu\text{S cm}^{-1}$ (Penna et al., 2014) and the pre-event water endmember as being equal to 95 $\mu\text{S cm}^{-1}$ (the mean value during baseflow conditions). Laudon and Slaymaker (1997), by investigating the hydrograph separation using EC at the lower station of an alpine catchment, defined the rainwater EC endmember as being equal to 6.15 $\mu\text{S cm}^{-1}$ and the pre-event water endmember as being equal to 39 $\mu\text{S cm}^{-1}$. However, young and old water EC endmembers are expected to be higher than event and pre-event water EC endmembers, respectively. Accordingly, these past results taken from the scientific literature support our assumption that $EC_{yw} < EC_{ow}$.

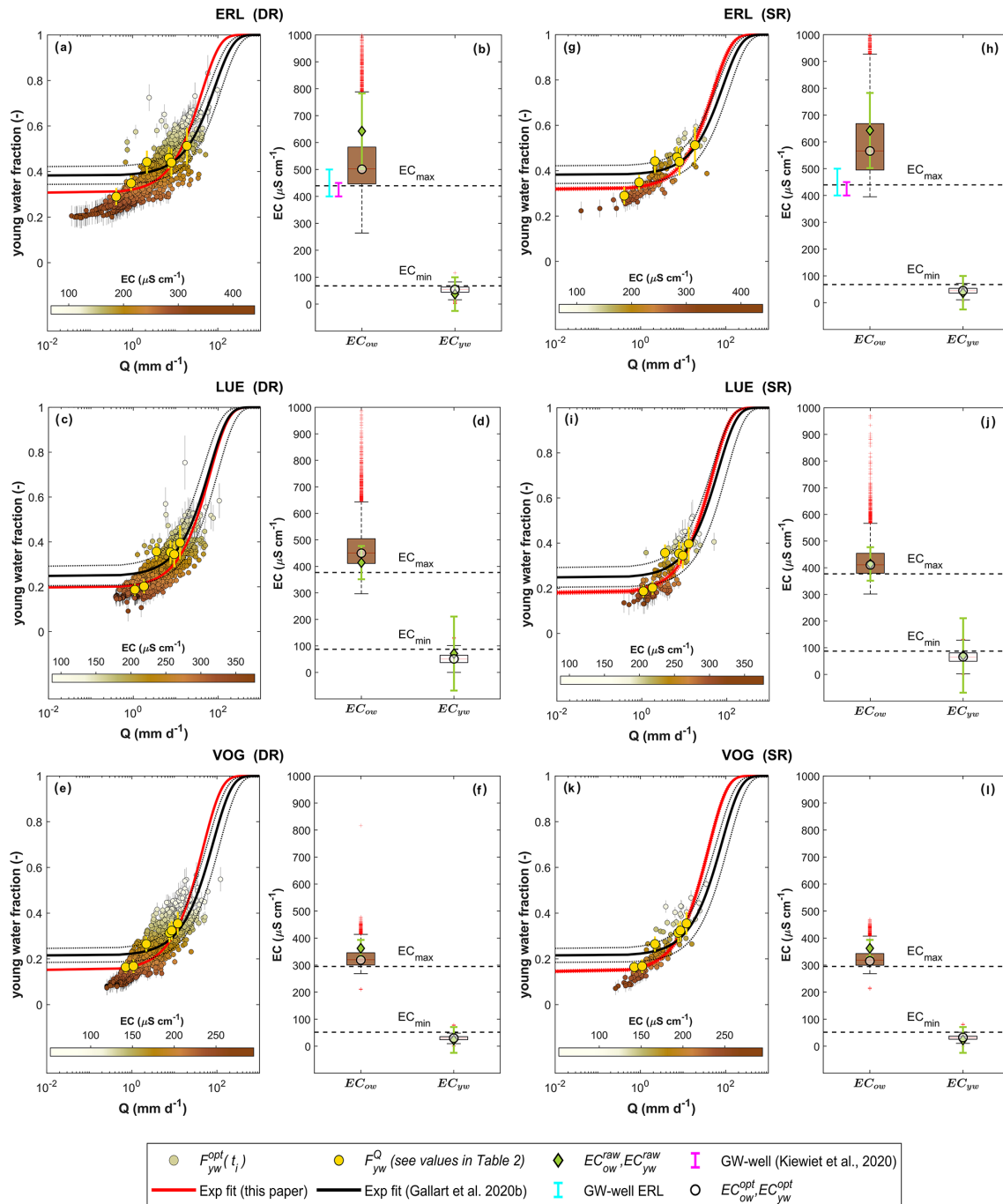


Figure 5. The $F_{yw}^{opt}(t_i)$ – $Q(t_i)$ relation for the ERL, LUE and VOG study catchments at the daily resolution (DR, **a**, **c**, **e**) and sampling resolution (SR, **g**, **i**, **k**) as well as the corresponding EC endmembers (**b**, **d**, and **f** and **h**, **j**, and **l**, respectively). The white–brown colour gradient of the $F_{yw}^{opt}(t_i)$ points indicates the $EC(t_i)$ value. For comparison, average F_{yw}^Q values of specific flow ranges (Table 2) are shown in yellow with related standard errors (yellow bars). The black curve represents the exponential-type fit using the parameters S_d^* and F_0^* previously obtained via non-linear fitting of Eq. (1) to stream water isotope data from Gallart et al. (2020b). The red curve represents the exponential-type fit using the parameters S_d^{EXP} and F_0^{EXP} obtained in this study via non-linear fitting of Eq. (10) to F_{yw}^{opt} vs. Q . Black and red dashed lines indicate ± 1 SE (standard error). Panels (**b**), (**d**), (**f**), (**h**), (**j**) and (**l**) show the box plots of EC_{yw}^{opt} and EC_{ow}^{opt} derived from the endmember uncertainty analysis. The white dots indicate the optimal endmembers (obtained by constraining the EC-based hydrograph separation using F_{yw} and F_{yw}^*) used to calculate $F_{yw}^{opt}(t_i)$ via Eq. (6). EC_{ow}^{raw} and EC_{yw}^{raw} (with the related SE values, green bars) have been superimposed for validation purposes along with the measured EC range in two groundwater wells within (solid cyan line) and near (solid magenta line) the ERL catchment. The dashed black lines, labelled EC_{max} and EC_{min} , refer to the respective maximum and minimum EC values measured in the stream.

The highest EC_{ow}^{opt} values were obtained for ERL ($501 \mu S cm^{-1}$, DR), whereas the lowest values were obtained for VOG ($319 \mu S cm^{-1}$, DR). The EC_{ow}^{opt} values are in line with those measured in groundwater (Fig. 5). In a 6.8 m deep monitoring well at the ERL meteorological station, groundwater EC generally varies between $400 \mu S cm^{-1}$ (spring–summer) and $500 \mu S cm^{-1}$ (fall–winter; data not shown), whereas the EC in groundwater at up to 1.5 m depth was generally around $400\text{--}450 \mu S cm^{-1}$ during no-snowmelt conditions in the neighbouring catchment of ERL (Kiewiet et al., 2020). The optimal endmembers are also in line with the first-order estimates of endmembers, EC_{ow}^{raw} and EC_{yw}^{raw} , derived from the exponential model fitted on median EC vs. F_{yw}^Q (Table 3; Figs. 3, 5), except for EC_{ow} in the ERL catchment. This can be explained by considering the high standard error (Table 3) of the parameter (corresponding to EC_{ow}^{raw}) in the exponential model that is poorly constrained for ERL (more than for LUE and VOG) at low young water fractions (Fig. 3). The optimized EC values of the young water fractions appear slightly elevated compared with data derived from central European precipitation (Monteith et al., 2023). However, it is plausible to posit that the young water fraction encompasses some soil water with higher EC.

Figure 5 shows further that the interquartile range (IQR) values of the EC_{ow}^{opt} empirical distributions are much larger than those of EC_{yw}^{opt} . Assuming that the solute concentration in stream water increases with water age (Riazi et al., 2022), this can possibly be explained by the much wider range of transit times (from approximately 0.2 to tending to infinity years) of old water compared with young water (0 to 0.2 years). Consequently, the concentrations of weathering-derived solutes in old water are not only higher but also more variable than in young water.

Our method estimates the EC endmember values for the cases $F_{yw}(t_i) = 1$ and $F_{yw}(t_i) = 0$ that are generally difficult to determine experimentally, thus providing additional information about young and old water in the systems under study. In this regard, at each one of the three study sites, the theoretical endmembers EC_{yw}^{opt} are lower than the minimum EC value measured in the streams; analogously, the calibrated EC_{ow}^{opt} values are higher than the maximum measured EC value (box plots vs. horizontal dashed lines in Fig. 5). This is expected for a natural, heterogeneous system in which incoming precipitation mixes with stored water, and thus stream water never contains 100 % young or 100 % old water. Instead, stream water is a mixture of these two components. This is supported by the fact that F_{yw}^Q values cover only a limited range of young water fractions (roughly from 0.1 to 0.5). This result demonstrates that the choice of the old water endmember based on tracer values sampled during base-flow conditions can result in an underestimation of the theoretical old water endmember. Although these stream conditions suggest the prevalence of old water, if the percentage of old water is less than 100 %, the measured tracers still reflect some mixing (albeit limited) with young water.

The estimated discharge sensitivity of the young water fraction, S_d^{EXP} , based on the EXPECT method satisfactorily describes the $F_{yw}^{opt}(t_i)\text{--}Q(t_i)$ relationships of the three catchments, as reflected by R^2 values of 0.58 and higher (Table 4; red curves in Fig. 5). Moreover, the red curve in Fig. 5 also fits the F_{yw}^Q values of the distinct flow regimes well (Table 2). By taking advantage of the consecutive $F_{yw}^{opt}(t_i)$ values at the daily or sampling resolution, we better constrain the parameters of Eq. (10) at very low and very high discharges compared with the fit obtained with Eq. (1) that is using only stream water $\delta^{18}O$ data at the sampling resolution (black curve in Fig. 5, Table 4; see the Supplement for methodological details). As a result, our estimated discharge sensitivity S_d^{EXP} is higher for the ERL and VOG catchments and similar (within error) for the LUE catchment compared to S_d^* , whereas our estimates of F_0^{EXP} for all three sites are slightly smaller than the respective F_0^* values obtained with Eq. (1).

We also find that the S_d^{EXP} values obtained at the SR can differ from those at the DR. For LUE, S_d^{EXP} at the SR is larger than at the DR (Table 4), whereas it is the other way around for ERL. Such differences can be attributed to the different flow regimes represented by the isotope samples that influence the EC endmember estimations at each site (Table 3). Moreover, at the DR, we are calibrating the EC endmembers using F_{yw} and F_{yw}^* based on isotope data at the SR. To be fully consistent in terms of the temporal resolution, we theoretically need daily stream water isotope data to derive F_{yw} and F_{yw}^* . The influence of sampling frequency is one of the limitations of the EXPECT method, as explained in Sect. 3.3. Nevertheless, the F_0^{EXP} values are consistent between the two temporal resolutions.

As can be seen in Fig. 5, the $F_{yw}^{opt}(t_i)$ values obtained with the EXPECT method form a data cloud around the idealized discharge sensitivity function of Eq. (10). Specifically, for a given discharge value, we obtain various $F_{yw}^{opt}(t_i)$ values, which can be explained by the delayed response of old water during precipitation events: while the young water fraction is generally highest during the rising limb of the hydrograph, it decreases during the falling limb when old water reaches the stream (von Freyberg et al., 2018a, b).

3.2 An immediate application of the EXPECT method: flow duration curves of young/old water and the temporal variability in the young water fractions

Because the EXPECT method allows for the estimation of the young water fraction $F_{yw}^{opt}(t_i)$ at up to the DR, we can determine the respective flow duration curves of young and old water discharge. Moreover, we calculate $Q_{50/50}$, i.e. the median discharge value at which 50 ± 1 % of both young and old water exist in streamflow. In the ERL catchment, Fig. 6a shows that a shift from old-water-dominated streamflow towards young water-dominated streamflow occurs for discharges larger than approximately 7.7 mm d^{-1} ($Q_{50/50}$;

Table 4. Comparison of discharge sensitivity parameters obtained with the EXPECT method (S_d^{EXP} and F_0^{EXP}), by fitting Eq. (10) to $F_{\text{yw}}^{\text{opt}}$ data (the goodness of fit is indicated by R^2), and parameters obtained with the Gallart et al. (2020b) method (S_d^* , F_0^*), by fitting Eq. (1) directly to the seasonal variation in the isotopic signal of stream water.

Time resolution	Catchment ID	$F_0^* \pm \text{SE} (-)$, Eq. (1) in Gallart et al. (2020b)	$F_0^{\text{EXP}} \pm \text{SE} (-)$, Eq. (10) in this study	$S_d^* \pm \text{SE} (\text{d mm}^{-1})$, Eq. (1) in Gallart et al. (2020b)	$S_d^{\text{EXP}} \pm \text{SE} (\text{d mm}^{-1})$, Eq. (10) in this study	R^2 in this study
Daily (DR)	ERL	–	0.3047 ± 0.002	–	0.024 ± 0.0005	0.62
	LUE	–	0.1948 ± 0.0016	–	0.0155 ± 0.0003	0.61
	VOG	–	0.1488 ± 0.0016	–	0.0211 ± 0.0004	0.64
Sampling (SR)	ERL	0.382 ± 0.0387	0.317 ± 0.0062	0.012 ± 0.0034	0.0198 ± 0.0016	0.64
	LUE	0.246 ± 0.0429	0.1773 ± 0.0073	0.016 ± 0.0056	0.0223 ± 0.0017	0.58
	VOG	0.214 ± 0.03	0.1415 ± 0.0056	0.012 ± 0.0036	0.0252 ± 0.0015	0.70

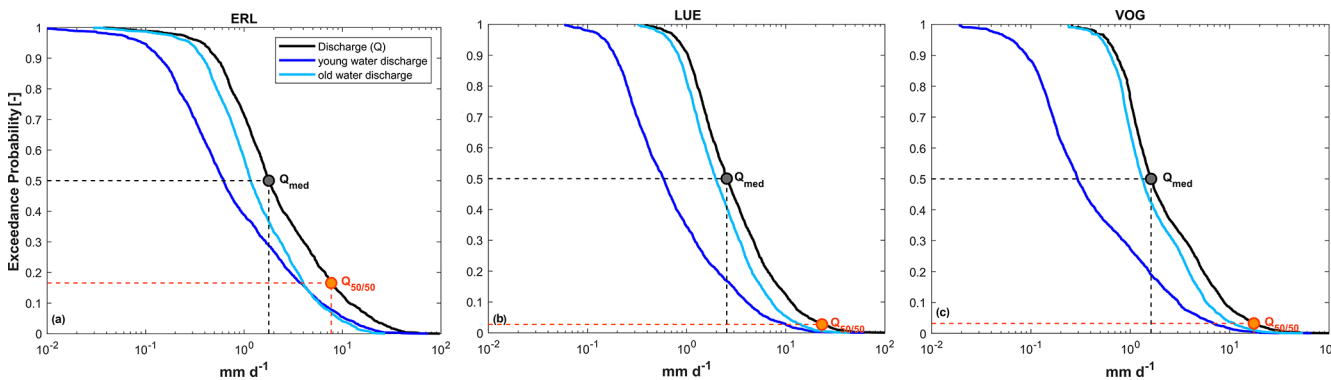


Figure 6. Total flow, young flow and old flow duration curves of the (a) ERL, (b) LUE and (c) VOG catchments. $Q_{50/50}$ indicates the median discharge value at which $50 \pm 1\%$ of both young and old water exists in streamflow. Q_{med} represents the median stream discharge.

Fig. 6a). In the LUE and VOG catchments, the streamflow contains more old water than young water for most of the flow regime (Fig. 6b, c); only on relatively few occasions, when Q exceeds $Q_{50/50}$ (23.2 and 17.5 mm d^{-1} , respectively), was the relative contribution of young water slightly larger than that of old water.

By comparing $Q_{50/50}$ with the median stream discharge (Q_{med}), we observe that $Q_{50/50}$ is higher than Q_{med} in all three study catchments (Fig. 6). This result suggests that a major proportion of old water reaches the stream more than 50% of the time. In both the LUE and VOG catchments, $Q_{50/50}$ is higher than in the ERL catchment, revealing that the LUE and VOG streams are dominated by old water for longer than the ERL stream. This explains why the isotope-based average young water fraction is higher in the ERL catchment than in the LUE and VOG catchments (Table 2).

With the EXPECT method, the temporal variability in $F_{\text{yw}}^{\text{opt}}(t_i)$ can be explored in detail, e.g. by comparing time series of $F_{\text{yw}}^{\text{opt}}(t_i)$ with those of other hydro-climatic variables (Fig. 7). Accordingly, in the following, we show a comparison between $F_{\text{yw}}^{\text{opt}}(t_i)$ and hydro-climatic observations at the DR of the ERL catchment, as it has the most

complete hydro-climatic data set (including discharge, precipitation, snow depth and temperature measurements; all data available from WSL) compared with the other two catchments. As visible from Fig. 7, daily young water fractions in the ERL catchment respond directly to precipitation events, which is further reflected by a strong positive correlation between $F_{\text{yw}}^{\text{opt}}(t_i)$ and the daily precipitation volumes ($\rho_{\text{Spearman}} = 0.41$, p value $\ll 0.01$ considering only days with precipitation; Fig. 8). We estimate that, after a rainfall or snowmelt event, the growth rate of $F_{\text{yw}}^{\text{opt}}(t_i)$ is on average $0.062 \pm 0.058 \text{ d}^{-1}$ (to reach the local $F_{\text{yw}}^{\text{opt}}(t_i)$ maximum next to the previous $F_{\text{yw}}^{\text{opt}}(t_i)$ local minimum; Fig. S1 in the Supplement). On the other hand, during the recession phase, the average rate of decrease in $F_{\text{yw}}^{\text{opt}}(t_i)$ is $-0.041 \pm 0.036 \text{ d}^{-1}$ (to reach the $F_{\text{yw}}^{\text{opt}}(t_i)$ local minimum next to the previous $F_{\text{yw}}^{\text{opt}}(t_i)$ local maximum; Fig. S1). Accordingly, $F_{\text{yw}}^{\text{opt}}(t_i)$ rapidly increases after an event (peak $F_{\text{yw}}^{\text{opt}}(t_i)$ is reached on average after $1.98 \pm 1.25 \text{ d}$), while it recedes slower during no-input days (the next minimum $F_{\text{yw}}^{\text{opt}}(t_i)$ is reached on average after $3.36 \pm 3.10 \text{ d}$). The largest daily young water fractions in the ERL catchment occurred during spring snowmelt (March–May), suggesting that the meltwater of the

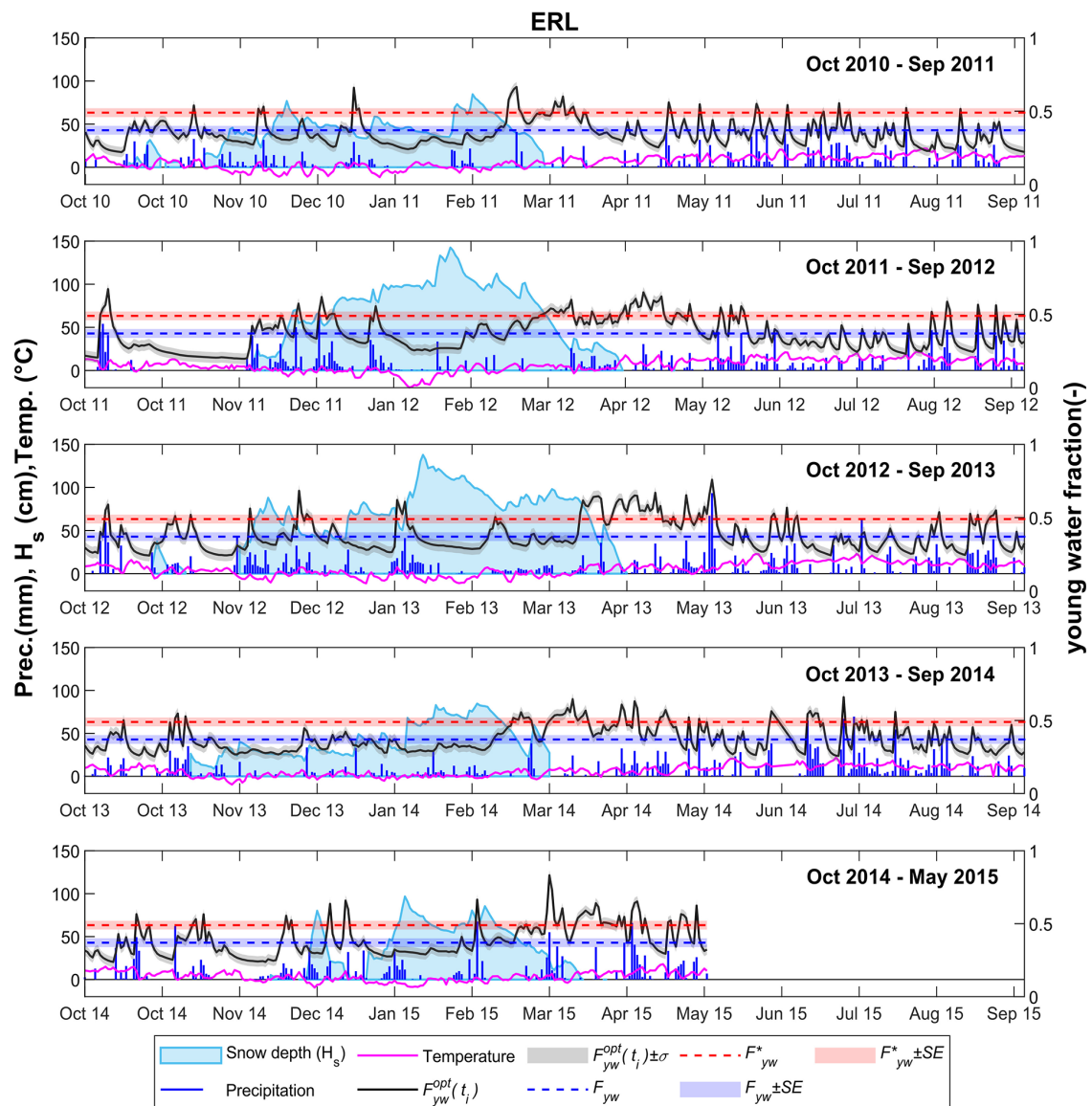


Figure 7. Time series of daily precipitation, snow depth, air temperature and F_{yw}^{opt} for the ERL catchment. Each panel reports a different hydrologic year.

ephemeral snowpack is an important source of young water (as no relevant water ageing is observed in such a snowpack) that flows off quickly in the stream (Gentile et al., 2023). Rapid surface runoff of snowmelt can occur due to soil freezing (temperatures $< 0^{\circ}\text{C}$) or high soil moisture contents (temperatures $> 0^{\circ}\text{C}$), both of which can limit infiltration (Harrison et al., 2021; Keller et al., 2017; Fig. 7). During the periods of snow accumulation and persistent snow cover, typically from November to February, $F_{yw}^{opt}(t_i)$ values were often as low as 0.3 and did not vary much (except during snowmelt and rain-on-snow events). Thus, streamflow in ERL was mainly composed of old water during this period, likely originating from the soil and groundwater storages.

3.3 Limitations of the EXPECT method and recommendations for future applications

While the EXPECT method can offer valuable insights into the young water fraction's discharge sensitivity and its temporal variability, it is not without its limitations. The assumption that EC is a proxy for stream water age may not hold true in all hydrological systems. For example, human activities, such as mining, irrigation or wastewater inputs can alter the stream water EC in unpredictable ways. Another example involves catchments with highly soluble rocks in the aquifers (e.g. limestone or gypsum) that are susceptible to dissolution by water. It has been shown that EC can increase with Q in some karst systems due to the remobiliza-

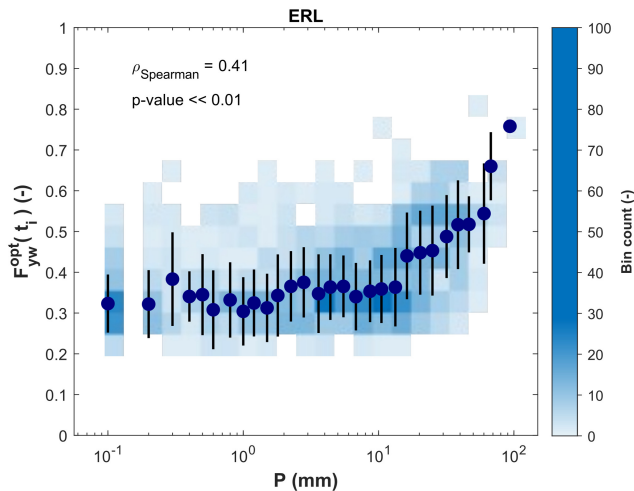


Figure 8. Correlation between daily F_{yw}^{opt} and daily precipitation when precipitation is higher than 0. Blue points indicate the median F_{yw}^{opt} observed in the stream corresponding to different ranges of daily precipitation with error bars indicating the standard deviation. These median F_{yw}^{opt} values are plotted against the median daily precipitation in each range. The blue colour gradient of the bins indicates the number of observations within each bin. A rapid increase in the young water fraction is observed when the daily precipitation is higher than 10 mm d^{-1} , reflecting hydrological connectivity and the generation of rapid flow paths.

tion of circulating water in the fractured areas (Balestra et al., 2022). Therefore, the F_{yw} –EC relationship (Eq. 3) can be very different from that in our three study catchments, which are mainly groundwater-influenced systems. Indeed, an early study also advised that one should be mindful of EC behaviour, as it depends on the specific characteristics of each catchment (Laudon and Slaymaker, 1997). Accordingly, for future applications of the method presented in this paper, we recommend visualization of the relationship between flow-specific young water fractions and flow-specific electrical conductivities with the aim of constructing a site-specific mixing relationship, as suggested by Kirchner (2016b). It should be noted that this relationship could potentially be different from an exponential mixing model. Indeed, the use of an exponential mixing model is not proposed to be the definitive answer to the problem of choosing the right mixing model for flow partitioning into young and old water. Accordingly, if the most suitable mixing model turns out to be different from an exponential mixing model, the equations presented in this study will need to be adapted to the specific case study. However, the method’s application scheme for calibrating the endmembers can still be employed. Nevertheless, in some catchments with short and sparse isotope time series, flow-specific young water fractions cannot be estimated reliably (von Freyberg et al., 2018b). The study by von Freyberg et al. (2018a) was able to estimate reliable flow-specific young water fractions for nine Swiss catchments that

comprised 4- to 5-year-long isotope time series with a minimum number of 81 samples to a maximum number of 140 samples, where stream water grab samples were collected approximately fortnightly. Thus, we suggest an isotope data set with these characteristics to construct a reliable site-specific mixing model with both flow-specific EC and F_{yw}^Q .

Another major limitation of the EXPECT method is its strong dependency on reliable F_{yw} and F_{yw}^* estimates, i.e. assumptions (ii) and (iii) in Sect. 2.2. If stream water isotope data sets are short or sparse, F_{yw} or F_{yw}^* can be highly uncertain and EC endmembers cannot be sufficiently constrained. Recently, Gallart et al. (2020a) revealed that unweighted and flow-weighted young water fractions were significantly lower than results with virtual (perfect) sampling when using a weekly sampling frequency. Thus, for the same catchment, we could potentially obtain different EC endmembers if stable water isotopes were sampled at higher or lower temporal resolution. Accordingly, we strongly recommend evaluating how the uncertainty in F_{yw} or F_{yw}^* propagates in the uncertainty in the calibrated endmembers, as described in Sect. 2.2.

For many catchments, Q and EC values are measured at a sub-hourly resolution. Thus, theoretically, the EXPECT method could provide reasonable young water fraction estimate results at these resolutions as well. However, we should consider that short-term variations in EC may not necessarily represent short-term variations in water age. For example, for a small stream in Sweden, Calles (1982) showed that diurnal variations in EC seem to be due to evapotranspiration but that the influence of gravity variations may also play a role. Moreover, a past study in a pre-alpine river in Switzerland revealed that the diurnal fluctuation in EC can be due to biogeochemical processes, such as calcite precipitation and photosynthesis (Hayashi et al., 2012). Accordingly, biological (photosynthesis and respiration) and chemical processes (carbonate equilibrium and calcite precipitation) can play a key role in controlling Ca^{2+} and HCO_3^- concentrations and, consequently, EC (Nimick et al., 2011; Hayashi et al., 2012). By calculating the average daily EC, and thus removing diurnal and nocturnal EC dynamics, it should better reflect variations in water age under the assumptions of the EXPECT method. Accordingly, we recommend applying the method using the daily mean of EC.

4 Summary and conclusions

The discharge sensitivity of the young water fraction (S_d^*) is a useful metric that quantifies how the proportion of stream-flow younger than 2–3 months changes as a catchment becomes wetter. In a past study, S_d^* was obtained by fitting a sine function to the stream water isotope values, assuming an exponential relationship between the young water fraction and discharge (Gallart et al., 2020b). Most available stream water isotope data sets are characterized by a relatively low

sampling frequency, which often fails to capture the entire flow regime from very low to very high discharges. This can result in highly uncertain or unrealistic estimates of the discharge sensitivity of young water fractions. Therefore, this paper aims to incorporate EC and $\delta^{18}\text{O}$ data to develop a new method that (a) estimates young water fractions at high temporal resolution by taking advantage of continuous EC measurements and (b) better constrains the estimated discharge sensitivity.

We have designed the EXPECT method that combines a sine-wave model of the seasonal isotope cycles and an alternative EC-based hydrograph separation. Specifically, we use an exponential mixing model in which EC endmembers are calibrated using unweighted and flow-weighted young water fractions obtained from $\delta^{18}\text{O}$ data. By considering the calibrated endmembers, daily and biweekly (sampling) young water fractions are estimated using EC measurements considered to be a proxy for the water age. The EXPECT method was tested in three small experimental catchments in Switzerland.

The application of this multi-tracer method has revealed that the optimal EC endmembers lie beyond the range of measured EC in stream water. This result reflects that streams are commonly a mixture of young and old water and that corresponding EC endmembers are difficult to obtain experimentally. The discharge sensitivities of the young water fractions obtained with the EXPECT method agree well with those obtained with the conventional approach, which uses only isotope data. However, the EXPECT method significantly reduced the standard error in the discharge sensitivity. In addition, the method allows for the estimation of young water fractions at a daily resolution, thereby providing interesting insights into short-term variations in the stream water age with changes in meteorological conditions, e.g. during snow accumulation and snowmelt. Young water fractions at a biweekly (i.e. sampling) resolution also revealed high reliability, highlighting the general applicability of this method in ungauged catchments: $\delta^{18}\text{O}$ and EC data can both be obtained from laboratory analysis of collected water samples, while Q can be directly measured in the stream during sampling campaigns using conventional methods (e.g. the current meter method or weir method) without the presence of fixed instrumentation for measuring Q and EC.

To conclude, a recent review paper (Benettin et al., 2022) highlighted the challenge of integrating non-conservative tracers in lumped models due to a missed definition of catchment-scale chemical properties. Overall, the EC for the three study catchments was found to be an informative property that keeps track, in an integrated way, of faster (younger) and slower (older) flow paths at the catchment scale. Considering the necessary precautions regarding the use of EC, the methodology presented in this paper can be applied (with possible adaptations) to other catchments to generate new insights into transit times, hydrologic flow paths and related sources.

Appendix A: Limitations of the linear mixing model

In order to use EC to separate the hydrograph into young and old water at a specified time t_i , we may employ the two-component EC-based hydrograph separation (ECHS), built on the water (Eq. A1) and tracer (Eq. A2) mass balance:

$$F_{yw}(t_i) + F_{ow}(t_i) = 1, \quad (\text{A1})$$

$$\text{EC}(t_i) = \text{EC}_{yw} F_{yw}(t_i) + \text{EC}_{ow} F_{ow}(t_i), \quad (\text{A2})$$

where $\text{EC}(t_i)$ is the electrical conductivity measured in the stream at the time t_i , EC_{yw} is the young water EC endmember and EC_{ow} is the old water EC endmember. By solving the system of two equations (Eqs. A1 and A2) with two variables ($F_{yw}(t_i)$ and $F_{ow}(t_i)$), we can obtain the explicit expression of $F_{yw}(t_i)$:

$$F_{yw}(t_i) = \frac{\text{EC}(t_i) - \text{EC}_{ow}}{\text{EC}_{yw} - \text{EC}_{ow}}. \quad (\text{A3})$$

As mentioned in Sect. 2.2, we assume $\text{EC}_{yw} < \text{EC}_{ow}$. However, by performing the constrained ECHS (Sect. 2.2), in which the two endmembers (EC_{yw} and EC_{ow}) are calibrated, the optimization algorithm finds $\text{EC}_{yw} = 0$, which is exactly the lower bound of the defined range $[0, +\infty)$ in which the optimization algorithm searches for the solution. This result suggests that the algorithm wants to search for the best solution below the lower bound of the specified range, thereby potentially returning a negative EC_{yw} value. This is consistent with the negative EC_{yw} obtained by fitting a linear model on the median EC vs. F_{yw}^Q of the three study catchments (Fig. 3). Obviously, this mathematical solution is not physically acceptable, but we can investigate this result to better understand the catchment functioning. Accordingly, if we make evaluate the expression of $\text{EC}(t_i)$ starting from Eq. (A3), we find a linear decrement of $\text{EC}(t_i)$ with the increasing $F_{yw}(t_i)$ (Eq. A4):

$$\begin{aligned} \text{EC}(t_i) &= (\text{EC}_{yw} - \text{EC}_{ow}) F_{yw}(t_i) + \text{EC}_{ow} \\ &= \alpha F_{yw}(t_i) + \text{EC}_{ow}. \end{aligned} \quad (\text{A4})$$

By requiring a negative EC_{yw} as the best solution, the constrained ECHS suggests that, for an exhaustive description of the catchments' behaviour, $\text{EC}(t_i)$ needs to rapidly decrease at low $F_{yw}(t_i)$, as shown by the red lines in Fig. A1. Nevertheless, physical reasons limit the slope (α) of this line ($\alpha \geq -\text{EC}_{ow}$); the most extreme, although still acceptable, condition (i.e. when $\text{EC}_{yw} = 0$ and $\alpha = -\text{EC}_{ow}$) is indicated by the dashed black line in Fig. A1a and b. Accordingly, to obtain a rapid decrease in $\text{EC}(t_i)$ at low $F_{yw}(t_i)$ and also maintain positive EC_{yw} , it is necessary to improve the linear mixing model. As visible from Fig. A1b, the exponential mixing model described in Sect. 2.2 was suitable to describe a rapid decrease in $\text{EC}(t_i)$ at low $F_{yw}(t_i)$ and maintain positive EC_{yw} .

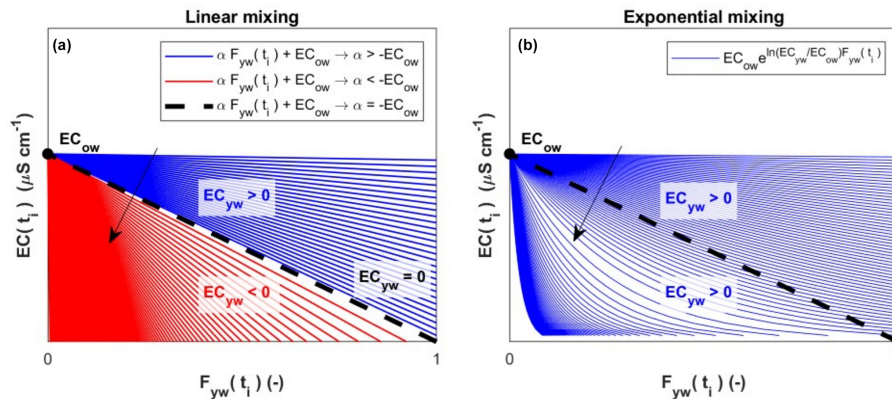


Figure A1. (a) Limits of the linear decay of $EC(t_i)$ with increasing $F_{yw}(t_i)$. Red lines with a slope (α) lower than $-EC_{ow}$ are not physically admitted because they imply a negative EC_{yw} ; (b) the exponential mixing overcomes this limit. Black arrows indicate the direction in which EC_{yw} decreases.

List of symbols.

*	Indicates a flow-weighted variable
a	Parameter of the exponential mixing model reported in Eq. (3)
A_p	Precipitation isotope cycle amplitude (‰) obtained via a volume-weighted robust fit of a sine function to the isotopic composition of precipitation
A_s	Stream water isotope cycle amplitude (‰) obtained via a robust fit of a sine function to the isotopic composition of stream water
A_s^*	Stream water isotope cycle amplitude (‰) obtained via a flow-weighted robust fit of a sine function to the isotopic composition of stream water
$A_s^*(Q)$	Stream water isotope cycle amplitude (‰) varying with discharge: $A_s^*(Q) = A_p F_{yw}^*(Q)$
A_s^Q	Stream water seasonal isotope cycles amplitude (‰) obtained by fitting sinusoids separately to the isotope data collected in different discrete flow regimes, as described in Kirchner (2016b) and von Freyberg et al. (2018a)
C_p	Isotopic composition of precipitation (‰)
C_s	Isotopic composition of stream water (‰)
DR	Daily resolution
EC	Electrical conductivity ($\mu\text{S cm}^{-1}$)
$EC(t_i)$	Electrical conductivity ($\mu\text{S cm}^{-1}$) in stream water at the generic time t_i
EC_{yw}	Young water electrical conductivity endmember ($\mu\text{S cm}^{-1}$)
EC_{yw}^{raw}	First-order estimate of the young water electrical conductivity endmember ($\mu\text{S cm}^{-1}$) obtained by evaluating the exponential model, fitted on the median-flow-specific EC vs. F_{yw}^Q , for $F_{yw}^Q = 1$
EC_{yw}^{opt}	Optimized young water electrical conductivity endmember ($\mu\text{S cm}^{-1}$) derived from calibration
EC_{ow}	Old water electrical conductivity endmember ($\mu\text{S cm}^{-1}$)
EC_{ow}^{raw}	First-order estimate of the old water electrical conductivity endmember ($\mu\text{S cm}^{-1}$) obtained by evaluating the exponential model, fitted on the median-flow-specific EC vs. F_{yw}^Q , for $F_{yw}^Q = 0$
EC_{ow}^{opt}	Optimized old water electrical conductivity endmember ($\mu\text{S cm}^{-1}$) derived from calibration
ECHS	EC-based hydrograph separation
ERL	Erlenbach catchment
EXPECT	Two-component electrical-conductivity-based hydrograph separation employing an EXPonential mixing model.

f	Frequency of the seasonal cycle (equal to once per year for a seasonal cycle)
F_{yw}	Unweighted average isotope-based young water fraction (–) obtained as A_S/A_P
\tilde{F}_{yw}	Unweighted average hydrograph-separation-based young water fraction (–) obtained with the exponential mixing model
F_{yw}^*	Flow-weighted average isotope-based young water fraction (–) obtained as A_S^*/A_P
\tilde{F}_{yw}^*	Flow-weighted average hydrograph-separation-based young water fraction (–) obtained with the exponential mixing model
$F_{yw}^*(Q)$	Young water fraction (–) varying with discharge following the exponential-type equation of Gallart et al. (2020b)
$F_{yw}(t_i)$	Young water fraction (–) at the generic time t_i
$F_{ow}(t_i)$	Old water fraction (–) at the generic time t_i
F_{yw}^{opt}	Optimized young water fractions (–), obtained with the exponential mixing model, using the calibrated endmembers EC_{yw}^{opt} and EC_{ow}^{opt}
$F_{yw}^{opt}(t_i)$	Optimized young water fraction (–) at the generic time t_i , obtained with the exponential mixing model, using the calibrated endmembers EC_{yw}^{opt} and EC_{ow}^{opt}
F_0^*	Virtual young water fraction (–) when $Q = 0$ in the exponential-type equation of Gallart et al. (2020b)
F_0^{EXP}	Virtual young water fraction (–) when $Q = 0$ obtained by fitting Eq. (6) of Gallart et al. (2020b) on F_{yw}^{opt} vs. Q data.
F_{yw}^Q	Young water fractions (–) estimated in discrete flow regimes as described in Kirchner (2016b) and von Freyberg et al. (2018a): $F_{yw}^Q = A_S^Q/A_P$
HS	Hydrograph separation
H_S	Snow depth (cm)
ID	Identifier
IHS	Isotope hydrograph separation
IQR	Interquartile range
k	Number (–) of precipitation isotope samples
k_S^*	Constant (‰) representing the vertical offset of the seasonal cycle
LUE	Lümpenbach catchment
n	Number (–) of Q and EC observations
m	Number (–) of stream water isotope samples
MTT	Mean transit time
obj	Objective function
Old water	Water with transit times roughly higher than 2–3 months (definition given in this paper)
P	Precipitation (mm)
$P(t_k)$	Volume of precipitation (mm) used for the volume-weighted fit of precipitation isotopes
q_1	1st quartile
q_2	2nd quartile
q_3	3rd quartile
Q	Discharge (mm d^{-1})
Q_{med}	Median stream discharge (mm d^{-1})
$Q(t_i)$	Discharge at the time t_i (mm d^{-1})
$Q(t_j)$	Discharge at the time t_j (mm d^{-1})
$Q_{50/50}$	Median discharge (mm d^{-1}) at which $50 \pm 1\%$ of both young and old water exists in streamflow
Young water	Water with transit times roughly lower than 2–3 months (definition given in this paper)
S_d^*	Discharge sensitivity of young water fraction (d mm^{-1}) obtained with the method of Gallart et al. (2020b)
S_d^{EXP}	Discharge sensitivity of young water fraction (d mm^{-1}) obtained by fitting Eq. (6) of Gallart et al. (2020b) on F_{yw}^{opt} vs. Q data
SE	Standard error
SR	Sampling resolution
t_i	Generic time in which Q and EC are measured
t_j	Generic time in which a stream water isotope sample is collected
t_k	Generic time in which a precipitation isotope sample is collected
VOG	Vogelbach catchment
$\delta^2\text{H}$	Isotope content (‰) considering deuterium
$\delta^{18}\text{O}$	Isotope content (‰) considering oxygen-18
$\delta^{18}\text{O}_p$	Isotope content of precipitation (‰) considering oxygen-18
$\delta^{18}\text{O}_p(t_k)$	Isotope content of precipitation (‰) at time t_k considering oxygen-18
$\delta^{18}\text{O}_s$	Isotope content of stream water (‰) considering oxygen-18
$\delta^{18}\text{O}_s(t_i)$	Isotope content of stream water (‰) at time t_i considering oxygen-18
φ_S^*	Phase of the seasonal cycle (rad)
σ	Standard deviation
ρ_{Spearman}	Spearman correlation coefficient

Data availability. Time series of $\delta^{18}\text{O}$ in streamflow and precipitation for the ERL, LUE and VOG catchments are available from Zenodo at <https://doi.org/10.5281/zenodo.4057967> (Staudinger et al., 2020b) and are presented and described in Staudinger et al. (2020a). Daily discharge and electrical conductivity data for the ERL, LUE and VOG catchments are available from the Swiss Federal Institute for Forest, Snow and Landscape research (WSL) data portal: <https://doi.org/10.16904/envidat.380> (Stähli, 2018). The shapefiles (.shp) for the ERL, LUE and VOG catchments are available from <https://doi.org/10.5281/zenodo.4057967> (Staudinger et al., 2020b).

Supplement. The supplement related to this article is available online at: <https://doi.org/10.5194/hess-28-1915-2024-supplement>.

Author contributions. AG, JvF and SF identified the research gap, designed the EXPECT method and prepared the paper. AG implemented the EXPECT method in a MATLAB code with support from DG and DC. All authors revised the manuscript and approved the submitted version.

Competing interests. The contact author has declared that none of the authors has any competing interests.

Disclaimer. Publisher's note: Copernicus Publications remains neutral with regard to jurisdictional claims made in the text, published maps, institutional affiliations, or any other geographical representation in this paper. While Copernicus Publications makes every effort to include appropriate place names, the final responsibility lies with the authors.

Acknowledgements. This work was supported by the PRIN MIUR 2017SL7ABC_005 WATZON Project, by the PRIN 2022 202295PFPK SUNSET Project and by Funding 2021 Fondazione CRT. Jana von Freyberg was supported by the Swiss National Science Foundation (SNSF; grant no. PR00P2_185931). The results of this study have been discussed within the COST Action WATSON, CA19120, supported by COST (European Cooperation in Science and Technology).

Financial support. This publication is part of the NODES project, which has received funding from the MUR – M4C2 1.5 of PNRR (grant no. ECS00000036).

Review statement. This paper was edited by Natalie Orlowski and reviewed by two anonymous referees.

References

- Balestra, V., Fiorucci, A., and Vigna, B.: Study of the Trends of Chemical–Physical Parameters in Different Karst Aquifers: Some Examples from Italian Alps, *Water*, 14, 441, <https://doi.org/10.3390/w14030441>, 2022.
- Benettin, P., Bailey, S. W., Campbell, J. L., Green, M. B., Rinaldo, A., Likens, G. E., McGuire, K. J., and Botter, G.: Linking water age and solute dynamics in streamflow at the Hubbard Brook Experimental Forest, NH, USA, *Water Resour. Res.*, 51, 9256–9272, <https://doi.org/10.1002/2015WR017552>, 2015.
- Benettin, P., Bailey, S. W., Rinaldo, A., Likens, G. E., McGuire, K. J., and Botter, G.: Young runoff fractions control streamwater age and solute concentration dynamics, *Hydrol. Process.*, 31, 2982–2986, <https://doi.org/10.1002/hyp.11243>, 2017.
- Benettin, P., Rodriguez, N. B., Sprenger, M., Kim, M., Klaus, J., Harman, C. J., van der Velde, Y., Hrachowitz, M., Botter, G., McGuire, K. J., Kirchner, J. W., Rinaldo, A., and McDonnell, J. J.: Transit Time Estimation in Catchments: Recent Developments and Future Directions, *Water Resour. Res.*, 58, e2022WR033096, <https://doi.org/10.1029/2022WR033096>, 2022.
- Bonacci, O. and Roje-Bonacci, T.: Water temperature and electrical conductivity as an indicator of karst aquifer: the case of Jadro Spring (Croatia), *Carbon. Evaporit.*, 38, 55, <https://doi.org/10.1007/s13146-023-00881-x>, 2023.
- Calles, U. M.: Diurnal Variations in Electrical Conductivity of Water in a Small Stream, *Hydrol. Res.*, 13, 157–164, <https://doi.org/10.2166/nh.1982.0013>, 1982.
- Camacho Suarez, V. V., Saraiva Okello, A. M. L., Wenninger, J. W., and Uhlenbrook, S.: Understanding runoff processes in a semi-arid environment through isotope and hydrochemical hydrograph separations, *Hydrol. Earth Syst. Sci.*, 19, 4183–4199, <https://doi.org/10.5194/hess-19-4183-2015>, 2015.
- Cano-Paoli, K., Chiogna, G., and Bellin, A.: Convenient use of electrical conductivity measurements to investigate hydrological processes in Alpine headwaters, *Sci. Total Environ.*, 685, 37–49, <https://doi.org/10.1016/j.scitotenv.2019.05.166>, 2019.
- Cey, E. E., Rudolph, D. L., Parkin, G. W., and Aravena, R.: Quantifying groundwater discharge to a small perennial stream in southern Ontario, Canada, *J. Hydrol.*, 210, 21–37, [https://doi.org/10.1016/S0022-1694\(98\)00172-3](https://doi.org/10.1016/S0022-1694(98)00172-3), 1998.
- Dansgaard, W.: Stable isotopes in precipitation, *Tellus*, 16, 436–468, <https://doi.org/10.3402/tellusa.v16i4.8993>, 1964.
- Gallart, F., Valiente, M., Llorens, P., Cayuela, C., Sprenger, M., and Latron, J.: Investigating young water fractions in a small Mediterranean mountain catchment: Both precipitation forcing and sampling frequency matter, *Hydrol. Process.*, 34, 3618–3634, <https://doi.org/10.1002/hyp.13806>, 2020a.
- Gallart, F., von Freyberg, J., Valiente, M., Kirchner, J. W., Llorens, P., and Latron, J.: Technical note: An improved discharge sensitivity metric for young water fractions, *Hydrol. Earth Syst. Sci.*, 24, 1101–1107, <https://doi.org/10.5194/hess-24-1101-2020>, 2020b.
- Gentile, A., Canone, D., Ceperley, N., Gisolo, D., Previati, M., Zuecco, G., Schaeffli, B., and Ferraris, S.: Towards a conceptualization of the hydrological processes behind changes of young water fraction with elevation: a focus on mountainous alpine catchments, *Hydrol. Earth Syst. Sci.*, 27, 2301–2323, <https://doi.org/10.5194/hess-27-2301-2023>, 2023.

- Harrison, H. N., Hammond, J. C., Kampf, S., and Kiewiet, L.: On the hydrological difference between catchments above and below the intermittent-persistent snow transition, *Hydrol. Process.*, 35, e14411, <https://doi.org/10.1002/hyp.14411>, 2021.
- Hayashi, M., Vogt, T., Mächler, L., and Schirmer, M.: Diurnal fluctuations of electrical conductivity in a pre-alpine river: Effects of photosynthesis and groundwater exchange, *J. Hydrol.*, 450–451, 93–104, <https://doi.org/10.1016/j.jhydrol.2012.05.020>, 2012.
- Hooper, R. P.: Diagnostic tools for mixing models of stream water chemistry, *Water Resour. Res.*, 39, 1055, <https://doi.org/10.1029/2002WR001528>, 2003.
- Keller, D. E., Fischer, A. M., Liniger, M. A., Appenzeller, C., and Knutti, R.: Testing a weather generator for downscaling climate change projections over Switzerland, *Int. J. Climatol.*, 37, 928–942, <https://doi.org/10.1002/joc.4750>, 2017.
- Kendall, C. and McDonnell, J. J.: *Isotope Tracers in Catchment Hydrology*, in: 1st Edn., Elsevier, 839 pp., ISBN 978-0-444-81546-0, 1998.
- Kiewiet, L., van Meerveld, I., Stähli, M., and Seibert, J.: Do stream water solute concentrations reflect when connectivity occurs in a small, pre-Alpine headwater catchment?, *Hydrol. Earth Syst. Sci.*, 24, 3381–3398, <https://doi.org/10.5194/hess-24-3381-2020>, 2020.
- Kirchner, J. W.: Aggregation in environmental systems – Part 1: Seasonal tracer cycles quantify young water fractions, but not mean transit times, in spatially heterogeneous catchments, *Hydrol. Earth Syst. Sci.*, 20, 279–297, <https://doi.org/10.5194/hess-20-279-2016>, 2016a.
- Kirchner, J. W.: Aggregation in environmental systems – Part 2: Catchment mean transit times and young water fractions under hydrologic nonstationarity, *Hydrol. Earth Syst. Sci.*, 20, 299–328, <https://doi.org/10.5194/hess-20-299-2016>, 2016b.
- Klaus, J. and McDonnell, J. J.: Hydrograph separation using stable isotopes: Review and evaluation, *J. Hydrol.*, 505, 47–64, <https://doi.org/10.1016/j.jhydrol.2013.09.006>, 2013.
- Laudon, H. and Slaymaker, O.: Hydrograph separation using stable isotopes, silica and electrical conductivity: an alpine example, *J. Hydrol.*, 201, 82–101, [https://doi.org/10.1016/S0022-1694\(97\)00030-9](https://doi.org/10.1016/S0022-1694(97)00030-9), 1997.
- Lazo, P. X., Mosquera, G. M., Cárdenas, I., Segura, C., and Crespo, P.: Flow partitioning modelling using high-resolution electrical conductivity data during variable flow conditions in a tropical montane catchment, *J. Hydrol.*, 617, 128898, <https://doi.org/10.1016/j.jhydrol.2022.128898>, 2023.
- McGuire, K. J. and McDonnell, J. J.: A review and evaluation of catchment transit time modeling, *J. Hydrol.*, 330, 543–563, <https://doi.org/10.1016/j.jhydrol.2006.04.020>, 2006.
- Meriano, M., Howard, K. W. F., and Eyles, N.: The role of midsummer urban aquifer recharge in stormflow generation using isotopic and chemical hydrograph separation techniques, *J. Hydrol.*, 396, 82–93, <https://doi.org/10.1016/j.jhydrol.2010.10.041>, 2011.
- Monteith, D. T., Henrys, P. A., Hruška, J., de Wit, H. A., Krám, P., Moldan, F., Posch, M., Ráike, A., Stoddard, J. L., Shilland, E. M., Pereira, M. G., and Evans, C. D.: Long-term rise in riverine dissolved organic carbon concentration is predicted by electrolyte solubility theory, *Sci. Adv.*, 9, eade3491, <https://doi.org/10.1126/sciadv.ade3491>, 2023.
- Mosquera, G. M., Segura, C., Vaché, K. B., Windhorst, D., Breuer, L., and Crespo, P.: Insights into the water mean transit time in a high-elevation tropical ecosystem, *Hydrol. Earth Syst. Sci.*, 20, 2987–3004, <https://doi.org/10.5194/hess-20-2987-2016>, 2016.
- Mosquera, G. M., Segura, C., and Crespo, P.: Flow Partitioning Modelling Using High-Resolution Isotopic and Electrical Conductivity Data, *Water*, 10, 904, <https://doi.org/10.3390/w10070904>, 2018.
- Nimick, D. A., Gammons, C. H., and Parker, S. R.: Diel biogeochemical processes and their effect on the aqueous chemistry of streams: A review, *Chem. Geol.*, 283, 3–17, <https://doi.org/10.1016/j.chemgeo.2010.08.017>, 2011.
- Pellerin, B. A., Wollheim, W. M., Feng, X., and Vörösmarty, C. J.: The application of electrical conductivity as a tracer for hydrograph separation in urban catchments, *Hydrol. Process.*, 22, 1810–1818, <https://doi.org/10.1002/hyp.6786>, 2008.
- Penna, D., Engel, M., Mao, L., Dell'Agnese, A., Bertoldi, G., and Comiti, F.: Tracer-based analysis of spatial and temporal variations of water sources in a glacierized catchment, *Hydrol. Earth Syst. Sci.*, 18, 5271–5288, <https://doi.org/10.5194/hess-18-5271-2014>, 2014.
- Penna, D., Engel, M., Bertoldi, G., and Comiti, F.: Towards a tracer-based conceptualization of meltwater dynamics and streamflow response in a glacierized catchment, *Hydrol. Earth Syst. Sci.*, 21, 23–41, <https://doi.org/10.5194/hess-21-23-2017>, 2017.
- Riazi, Z., Western, A. W., and Bende-Michl, U.: Modelling electrical conductivity variation using a travel time distribution approach in the Duck River catchment, Australia, *Hydrol. Process.*, 36, e14721, <https://doi.org/10.1002/hyp.14721>, 2022.
- Schmidt, C., Musolff, A., Trauth, N., Vieweg, M., and Fleckenstein, J. H.: Transient analysis of fluctuations of electrical conductivity as tracer in the stream bed, *Hydrol. Earth Syst. Sci.*, 16, 3689–3697, <https://doi.org/10.5194/hess-16-3689-2012>, 2012.
- Stähli, M.: Longterm hydrological observatory Alptal (central Switzerland), *EnviDat* [data set], <https://doi.org/10.16904/envidat.380>, 2018.
- Stähli, M., Seibert, J., Kirchner, J. W., von Freyberg, J., and van Meerveld, I.: Hydrological trends and the evolution of catchment research in the Alptal valley, central Switzerland, *Hydrol. Process.*, 35, e14113, <https://doi.org/10.1002/hyp.14113>, 2021.
- Staudinger, M., Stoelzle, M., Seeger, S., Seibert, J., Weiler, M., and Stahl, K.: Catchment water storage variation with elevation, *Hydrol. Process.*, 31, 2000–2015, <https://doi.org/10.1002/hyp.11158>, 2017.
- Staudinger, M., Seeger, S., Herbstritt, B., Stoelzle, M., Seibert, J., Stahl, K., and Weiler, M.: The CH-IRP data set: a decade of fortnightly data on $\delta^2\text{H}$ and $\delta^{18}\text{O}$ in streamflow and precipitation in Switzerland, *Earth Syst. Sci. Data*, 12, 3057–3066, <https://doi.org/10.5194/essd-12-3057-2020>, 2020a.
- Staudinger, M., Seeger, S., Herbstritt, B., Stoelzle, M., Seibert, J., Stahl, K., and Weiler, M.: The CH-IRP data set: fortnightly data of $\delta^2\text{H}$ and $\delta^{18}\text{O}$ in streamflow and precipitation in Switzerland (Version 2), *Zenodo* [data set], <https://doi.org/10.5281/zenodo.4057967>, 2020b.
- von Freyberg, J., Allen, S. T., Seeger, S., Weiler, M., and Kirchner, J. W.: Sensitivity of young water fractions to hydro-climatic forcing and landscape properties across 22 Swiss catchments, *Hydrol. Earth Syst. Sci.*, 22, 3841–3861, <https://doi.org/10.5194/hess-22-3841-2018>, 2018a.

- von Freyberg, J., Studer, B., Rinderer, M., and Kirchner, J. W.: Studying catchment storm response using event- and pre-event-water volumes as fractions of precipitation rather than discharge, *Hydrol. Earth Syst. Sci.*, 22, 5847–5865, <https://doi.org/10.5194/hess-22-5847-2018>, 2018b.
- Wang, L., von Freyberg, J., van Meerveld, I., Seibert, J., and Kirchner, J. W.: What is the best time to take stream isotope samples for event-based model calibration?, *J. Hydrol.*, 577, 123950, <https://doi.org/10.1016/j.jhydrol.2019.123950>, 2019.
- Xia, C., Zuecco, G., Chen, K., Liu, L., Zhang, Z., and Luo, J.: The estimation of young water fraction based on isotopic signals: challenges and recommendations, *Front. Ecol. Evol.*, 11, 1114259, <https://doi.org/10.3389/fevo.2023.1114259>, 2023.
- Zuecco, G., Penna, D., and Borga, M.: Runoff generation in mountain catchments: long-term hydrological monitoring in the Rio Vauz Catchment, Italy, *Cuad. Investig. Geográfica*, 44, 397–428, <https://doi.org/10.18172/cig.3327>, 2018.